

LA-UR-17-31351

Approved for public release; distribution is unlimited.

Title: Summary of a Gas Transport Tracer Test in the Deep Cerros Del Rio Basalts, Mesita del Buey, Los Alamos NM.

Author(s): Stauffer, Philip H.
Rahn, Thomas A.
Ortiz, John Philip
Salazar, Larry Joseph
Boukhalfa, Hakim
Snyder, Emily Elisabeth

Intended for: Report

Issued: 2018-01-16 (rev.1)

Disclaimer:

Los Alamos National Laboratory, an affirmative action/equal opportunity employer, is operated by the Los Alamos National Security, LLC for the National Nuclear Security Administration of the U.S. Department of Energy under contract DE-AC52-06NA25396. By approving this article, the publisher recognizes that the U.S. Government retains nonexclusive, royalty-free license to publish or reproduce the published form of this contribution, or to allow others to do so, for U.S. Government purposes. Los Alamos National Laboratory requests that the publisher identify this article as work performed under the auspices of the U.S. Department of Energy. Los Alamos National Laboratory strongly supports academic freedom and a researcher's right to publish; as an institution, however, the Laboratory does not endorse the viewpoint of a publication or guarantee its technical correctness.

A Gas Transport Tracer Test in the Deep Cerros Del Rio Basalts, Mesita del Buey, Los Alamos NM.

Philip H. Stauffer¹, Thom Rahn², John P. Ortiz¹, Larry Salazar³, Hakim Boukalfa², and Emily Snyder^{1,4}

¹EES-16, ²EES-14, ³ER- Field Services, ⁴New Mexico Institute of Mining and Technology

Table of Contents

1	Introduction	4
1.1	Background	5
1.2	Borehole 54-24399	6
2	Pre-test Numerical Modeling.....	11
2.1	Model Domain and Boundary Conditions.....	11
2.2	Pre-test simulation results	11
3	Tracer Experiment Details.....	13
3.1	Analytical Instruments	13
3.2	Analytical and Field Methods.....	15
3.3	Noble Gas Tracer.....	18
3.4	Pressure and Temperature Measurements.....	18
3.5	Preliminary Test in December of 2016	19
3.6	April 2017 Tracer Tests	20
3.6.1	Injection and Sampling at 566.7 ft bgs.....	20
3.6.2	Injection and Sampling at 587.8 ft bgs.....	21
3.7	Sampling at Secondary Wells	22
4	Results from the April 2017 Tracer Test	22
4.1	Pressure Results.....	22
4.2	INNOVA Results.....	23
4.2.1	Data Gaps	23
4.2.2	Sulfur Hexafluoride Results.....	24
4.2.3	1,1,1-TCA and PCE Results	25
4.3	QMS results.....	27
5	Post-Test Analytical Analysis and Scoping Calculations.....	28
5.1	Analytical Analysis.....	28
5.2	Scoping Calculations	30
6	Post-Test Numerical Modeling.....	32
6.1	Model Domain	32
6.2	Material Properties	33
6.3	Boundary Conditions.....	34
6.4	Estimating in situ Dispersivity	35
7	Discussion.....	38

7.1	Borehole 54-24399 Data Variability.....	38
7.2	Revised Conceptual Model	39
8	References	41
9	Appendix A: FEHM Input Files.....	43
9.1	FEHM Input Deck	43
9.2	Zone file for the location of the atmospheric boundary and basalt regions.....	46
9.3	FEHMN.FILES.....	47
10	Appendix B: Tracer Test Implementation Details	47

Table of Figures

Figure 1.1-1	Site map of MDA L including borehole 54-24399 (BH-B) and angled boreholes 54-01015 and 54-01016.	6
Figure 1.1-2	Stratigraphy beneath MDA L.	6
Figure 1.1-3	Pressure variation in the Cerros del Rio basalt relative to the overlying Bandelier Tuff (Neeper 2002, Figure 8)	6
Figure 1.2-1	New permanent packer installed in borehole 54-24399 in August 2017.....	7
Figure 1.2-2	Nitrogen supply including pressure reduction valve.	8
Figure 1.2-3	Surface completion for borehole 54-24399.	8
Figure 1.2-4	Top of the permanent packer showing the OMEGA pressure transducer, one sample line and the nitrogen inflation line.	9
Figure 1.2-5	Schematic of the completed single packer installation in borehole 54-24399.	10
Figure 2.2-1	Pre-experiment numerical domain for tracer test simulations.....	12
Figure 2.2-2	Pre-experiment predicted concentration in the open borehole (54-24399) versus time, for diffusion only and barometrically pumped dispersion.....	12
Figure 3.1-1	Innova 1412i Photoacoustic Gas Monitor, installed in the field at MDA L, April 2017.	14
Figure 3.1-2	OmniStar™ Quadrapole Mass Spectrometer.....	14
Figure 3.1-3	INNOVA calibration to LANL created SF ₆ standards	15
Figure 3.1-4	QMS calibration to LANL created SF ₆ standards.....	15
Figure 3.2-1	10-L Carboy used as a gas reservoir to ensure continuous INNOVA operation.	17
Figure 3.2-2	Field equipment tower.	17
Figure 3.2-3	Wellhead with sampling lines connected to desiccant	18
Figure 3.4-1	Campbell Scientific Data Logger CR5000 and 10 amp power supply.	19
Figure 3.5-1	Pressure during the Dec. 2016 preliminary tracer test	20
Figure 3.5-2	Timing of SF ₆ injections, measured SF ₆ , and temperature during the Dec. 2016 preliminary tracer test.....	20
Figure 3.6-1	Schematic of sampling train at the surface of borehole 54-24399.	21
Figure 4.1-1	Measured surface pressure at MDA L, April 3-17, 2017.....	22
Figure 4.1-2	Measured surface pressure adjusted to the same mean value as measured downhole pressure at 566.7 ft bgs.	23

Figure 4.1-3 Measured pressure differential between surface and downhole (566.7 ft bgs) for April 3-17, 2017.	23
Figure 4.2-1 Subsurface CO ₂ as an indicator of data quality.....	24
Figure 4.2-2 SF ₆ data collected with the INNOVA from April 5 – 17, 2017.....	25
Figure 4.2-3 INNOVA measures (gold) of 1,1,1-TCA concentration from borehole 54-24399 during 12 days in April 2017. Pressure measured beneath the packer is also shown (red).....	26
Figure 4.2-4 INNOVA measures (gold) of 1,1,1-TCA concentration from borehole 54-24399 during 12 days in April 2017. Measured surface temperature is also shown (red).....	26
Figure 4.2-5 INNOVA measures of PCE (gold) from borehole 54-24399 during 12 days in April 2017. Measured surface temperature is also shown (red).....	27
Figure 4.3-1 SF ₆ (gold) and surface temperature (red) versus time for the QMS.....	28
Figure 5.1-1 Spectral density	29
Figure 5.1-2 Schematic of the domain. Distance from wellbore to atmosphere is x.	29
Figure 5.2-1 FEHM pressure responses with varying global tolerances compared to the analytical solution.	31
Figure 6.1-1 Model domain schematic, X-Z plane. Sampling ports are shown in red.	33
Figure 6.1-2 Model domain schematic Y direction.	33
Figure 6.3-1 Measured atmospheric pressure, March 5 – April 17 at TA-54, simulated atmospheric pressure boundary, and measured downhole pressure beneath the packer in borehole 54-24399 at 566.7 ft bgs.	34
Figure 6.3-2 Data versus simulation results at 566.7 ft bgs for SF ₆ concentration and pressure.....	35
Figure 6.4-1 Dispersion coefficient as a function of time for both the rubblized basalt (blue) and the massive fractured basalt (red).....	37
Figure 6.4-2 Average linear velocity as a function of time in the rubblized basalt (blue) and the massive fractured basalt (red).....	37
Figure 7.1-1 SUMMA data for 1,1,1-TCA for borehole 54-24399	38
Figure 7.1-2 Conceptual model for transport in the Cerros del Rio Basalt.....	39

1 Introduction

Here we describe results from a tracer test in the Cerros del Rio basalt beneath Mesita del Buey, Technical Area 54 (TA-54) at Los Alamos National Laboratory (LANL or the Laboratory). This report follows from plans outlined in our previous Tracer Test Work Plan (LANL 2016). These activities were conducted by LANL to further characterize subsurface properties of the Cerros del Rio basalts at Material Disposal Area (MDA) L (Figure 1.1-1). The work presented follows from the “Interim Measures Work Plan for Soil-Vapor Extraction of Volatile Organic Compounds from Material Disposal Area L, Technical Area 54, Revision 1,” submitted to the New Mexico Environment Department (NMED) in September 2014 (LANL 2014). Remediation of the MDA L vapor plume by soil-vapor extraction (SVE) is recommended as part of the final remedy in the “Corrective Measures Evaluation Report for Material Disposal Area L, Solid Waste Management Unit 54-006, at Technical Area 54, Revision 2” to meet a remedial action objective of preventing groundwater from being impacted above a regulatory standard by the transport of volatile organic compounds (VOCs) to groundwater through soil vapor (LANL 2011).

The depth to regional groundwater beneath MDA L is on the order of 285 m (935 ft), whereas the vapor plume is predominantly within the Bandelier Tuff in the upper 90 m (300 ft) of the surface. The tuff units beneath the surface at MDA L are underlain by a thick (nearly 150 m [500 ft]) sequence of Cerros del Rio basalts (Figure 1.1-2). Although transport within the Bandelier Tuff is fairly well understood, there remains considerable uncertainty regarding the long-term transport of vapors downward through the Cerros del Rio basalt towards the regional aquifer and/or towards basalt outcrops in White Rock Canyon.

1.1 Background

To further characterize subsurface properties in the Cerros del Rio basalt, the Laboratory undertook a gas tracer test that has provided data to determine diffusivity in the fractured basalt that makes up nearly half the thickness of the unsaturated rock column between the MDA L disposal area and the regional water table (Figure 1.1-2). The tracer testing provides fundamental gas flow and transport information under field conditions that would otherwise be difficult to obtain. In particular, an objective of the tracer test was to investigate the effects of changes in atmospheric pressure on the mobility of deep gaseous contaminants, a phenomenon known as barometric (or atmospheric) pumping.

Theoretical and numerical reasoning combined with field observations have led to the conclusion that barometric pumping in the Cerros del Rio basalt will likely lead to 1–2-kPa variations in subsurface pressure (Neeper 2002). Such pressure variations will induce oscillatory flow and create an effective diffusivity that could be orders of magnitude larger than pure gas diffusion (Auer et al. 1996). Field measurements have shown that the pressure variations in the basalt are damped less than pressure variations in the overlying tuff (Figure 1.1-3). This indicates that the basalt is extremely conductive to air flow from outcrops such as those seen in White Rock Canyon to the east of MDA L.

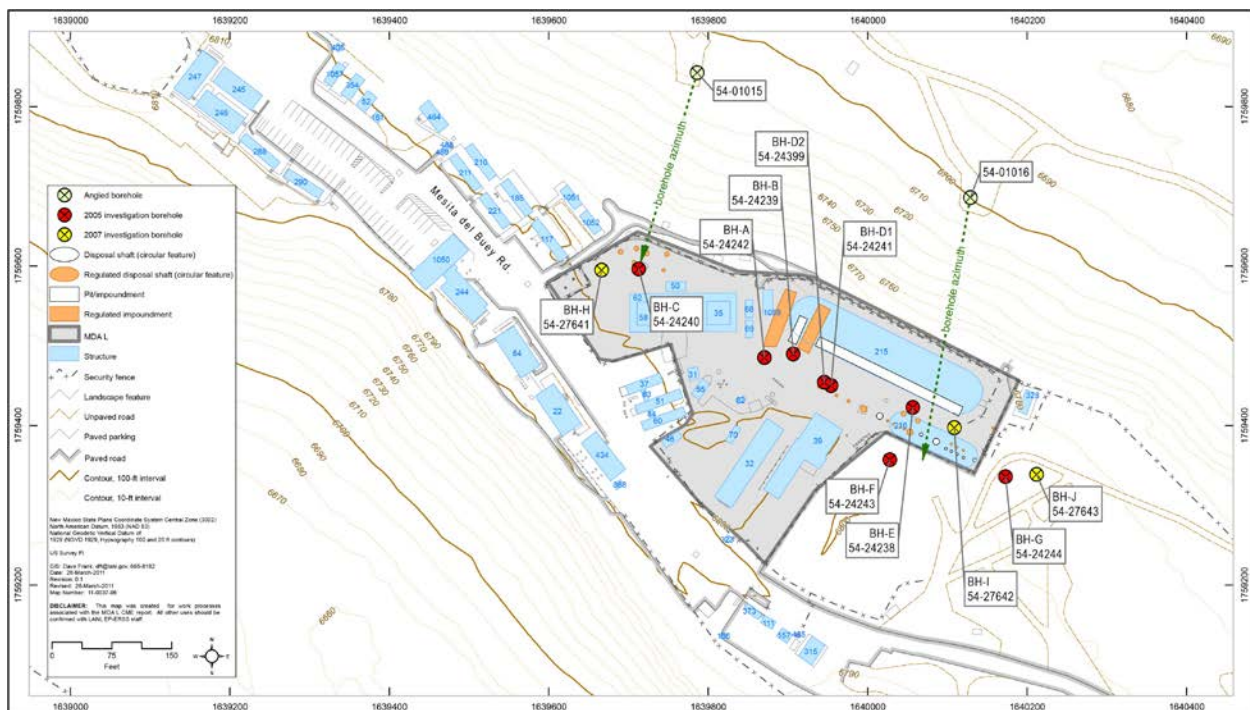


Figure 1.1-1 Site map of MDA L including borehole 54-24399 (BH-B) and angled boreholes 54-01015 and 54-01016.

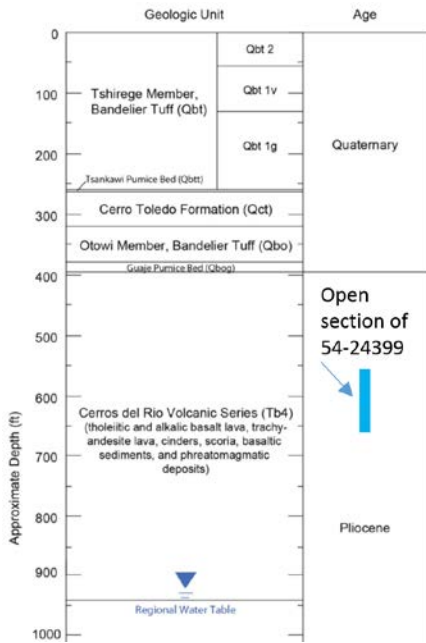


Figure 1.1-2 Stratigraphy beneath MDA L.

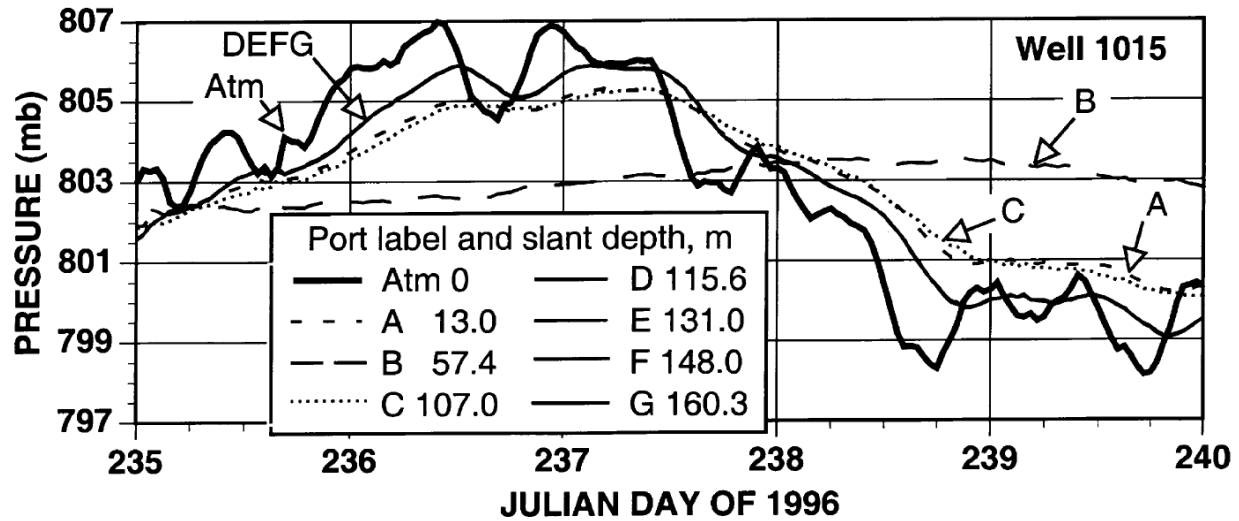


Figure 1.1-3 Pressure variation in the Cerros del Rio basalt relative to the overlying Bandelier Tuff (Neeper 2002, Figure 8)

1.2 Borehole 54-24399

Borehole 54-24399 was installed in 2005 near the center of MDA L (Figure 1.1-1) and has been used to sample the VOC plume concentrations in the Cerros del Rio basalt. A dedicated packer system and sampling line are used to collect samples at borehole 54-24399. In the past, a drill rig was used for

lowering and raising the packer system into the borehole. Due to issues with packer destruction on sharp basalt, the decision was made by LANL to install a single permanent packer (Figure 1.2-1).

The permanent packer was placed with its bottom at 566.7 ft bgs within the casing of the wellbore. To sample 54-24399, the packer is inflated with pure nitrogen (99.99%) from a surface port to the desired inflation pressure according to the manufacturer's specification (50 psi). The nitrogen is supplied from a large 2000 psi tank coupled to a pressure reducer (Figure 1.2-2). The sample train is then connected to one of the two ports on the new surface completion (Figure 1.2-3). The new packer has two sample ports, one pulling air from 566.7 ft bgs and one pulling air from 587.7 ft bgs. The port labeled SAMPLE in Figure 1.2-3 is open to 587.7 ft bgs while the port labeled TRACER is open to 566.7 ft bgs. There is also an OMEGA (PX429-015AI-EH) extra high accuracy 0-15 psi ($\pm 0.05\%$) pressure transducer mounted on the top of the packer that is open to a port at 566.7 ft bgs (Figure 1.2-4). This transducer is connected to the surface through a grey wire shown in Figure 1.2-3 that can be attached to a data logger. The pressure transducer is used to demonstrate the close coupling between the atmosphere and the subsurface pressure within the basalt. A schematic of the new completion is shown in Figure 1.2-5 and includes rock types as seen in a video log of the borehole. The depth of the second, deeper port beneath the packer is 587.7 ft. bgs.



Figure 1.2-1 New permanent packer installed in borehole 54-24399 in August 2017.



Figure 1.2-2 Nitrogen supply including pressure reduction valve.



Figure 1.2-3 Surface completion for borehole 54-24399.



Figure 1.2-4 Top of the permanent packer showing the OMEGA pressure transducer, one sample line and the nitrogen inflation line.

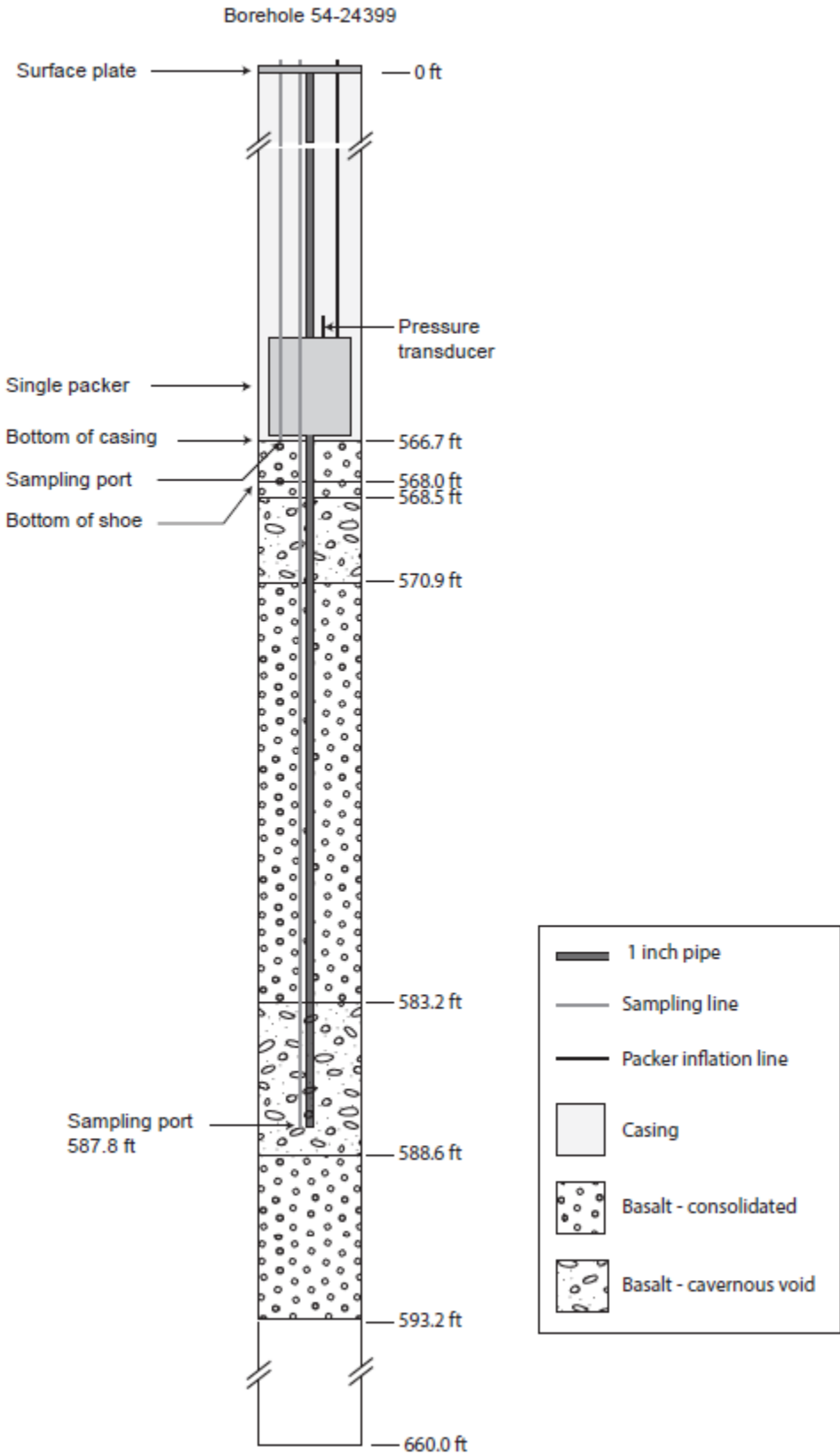


Figure 1.2-5 Schematic of the completed single packer installation in borehole 54-24399.

2 Pre-test Numerical Modeling

Prior to the experiment, to demonstrate the process of barometric pumping, a numerical model representing a 90-ft section of uncased borehole located at the center of a two-dimensional radial domain was developed. The model is built within FEHM (Finite Element Heat and Mass) porous-flow simulator, which was developed at the Laboratory and has been used successfully to simulate barometrically pumped contaminant transport in fractured rock (Neeper and Stauffer 2012A and 2012B; Jordan et al., 2014 and 2015).

2.1 Model Domain and Boundary Conditions

The domain includes layers of both vesicular and massive basalt extending from the top of the basalt at 118 m (388 ft) below ground surface (bgs) to a depth of approximately 290 m (950 ft) bgs based on borehole geophysical logs for well 54-24399 (Figure 2.2-1). Vesicular basalt and massive basalt are assigned porosity values of 35% and 0.1%, respectively. Permeability of these units is based on the work of Neeper (2002), where a best fit to amplitude and phase-shift of pressure data from boreholes 54-1015 and 54-1016 yielded a permeability/porosity ratio of $2.2 \times 10^{-8} \text{ m}^2$. The domain is initialized with an average mesa pressure of 80 kPa, and a barometric pressure wave obtained from August 2015 Technical Area 54 (TA-54) atmospheric data is applied to the outer boundary at a radius of 1.5 km (0.9 mi) based on Neeper (2002). In the numerical model, we assume a packer will isolate pressure within a 27-m (90-ft) section of uncased borehole. An initial tracer concentration of 200 ppmv is applied to the simulated borehole nodes, which corresponds to an initial tracer mass of approximately 0.5 g of SF_6 (Figure 2.2-1).

2.2 Pre-test simulation results

Figure 2.2-2 shows concentration versus time within the open borehole for a simulation of gas tracer transport for a case with an initial low in the barometric pressure applied at the outer boundary of the radial domain compared with a simulation with diffusion only. For the diffusion-only case, the tracer mass initially located in the open borehole moves radially outward along a concentration gradient. Concentrations within the borehole monotonically decrease with time. This curve is an end-member of possible behavior if the permeability in the basalt were not connected to the atmosphere. For the case where the basalt permeability is well connected to the atmosphere, the results are dramatically different. The initial low pressure in the atmospheric-pressure wave causes the tracer mass (0.5 g of SF_6) in the open borehole to rapidly move radially out of the borehole into the formation, thereby reducing concentrations at very early times. However, because atmospheric pressure soon increases to values above average, flow is reversed and the tracer is pushed back into the open borehole. Simultaneously, the tracer mixes with pore gas, leading to rapid dilution and a decrease in the concentration measurable in the open borehole. These two curves represent potential extremes of the system behavior, and data from the proposed tracer test will allow the Laboratory to make the first in situ estimates of barometrically enhanced diffusion in the Cerros del Rio basalts.

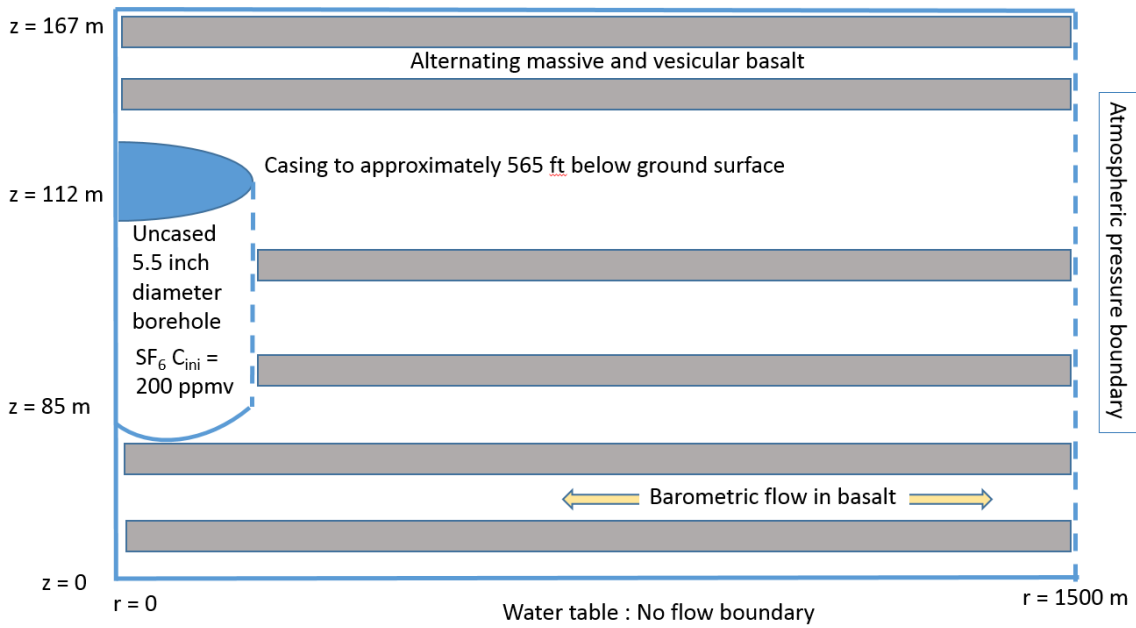


Figure 2.2-1 Pre-experiment numerical domain for tracer test simulations.

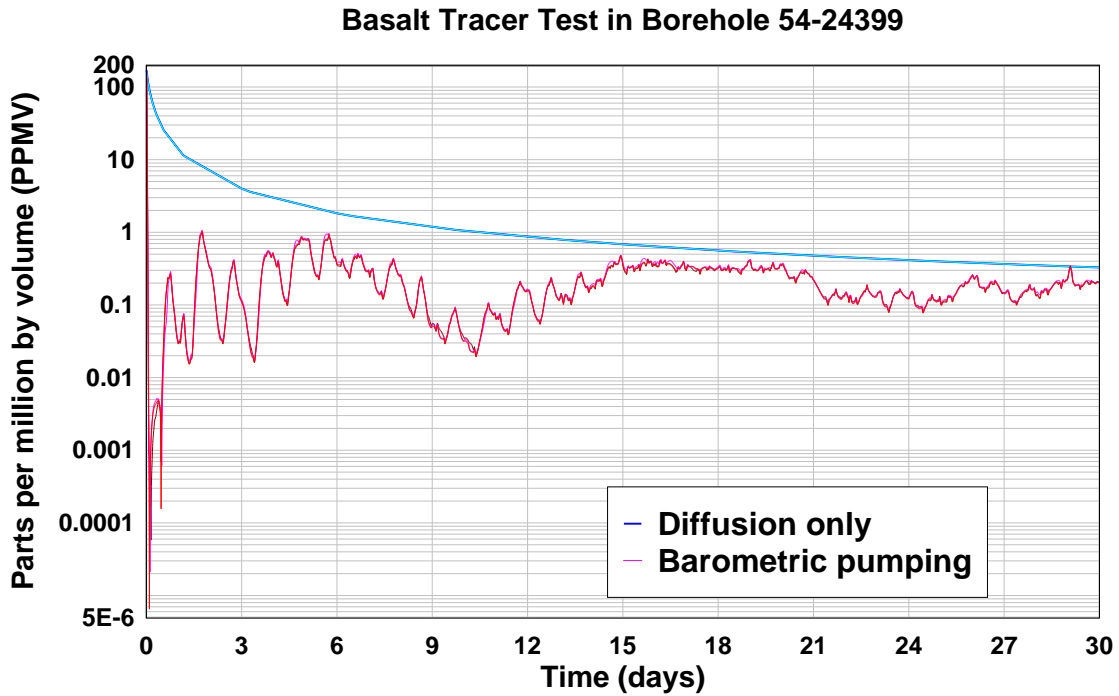


Figure 2.2-2 Pre-experiment predicted concentration in the open borehole (54-24399) versus time, for diffusion only and barometrically pumped dispersion

3 Tracer Experiment Details

Preliminary activities for the tracer experiment included planning, analysis of existing data, and training of personnel. The tracer test included injections of gas tracers (SF_6 , neon, and krypton) into borehole 54-24399 through a single packer system and subsequent monitoring of concentration decay as the tracer spread into the subsurface. SF_6 is an inorganic, colorless, odorless, nonflammable gas that is poorly soluble in water. Borehole 54-24399 is cased from ground surface to a depth of 565 ft, followed by an uncased section of approximately 28 m (92 ft). This borehole was chosen because it is the only borehole at MDA L that has an uncased section open in the Cerros del Rio basalt. The proposed SF_6 mass to be injected into the uncased section of borehole was initially planned to be 0.5 g per test injection, based on maintaining a total tracer mass fraction of less than 0.1% to ensure no density-driven flow. However, during initial work in December of 2016, the project found that these small tracer amounts yielded an analytical signal near the lower threshold of the photoacoustic analytical system requiring subsequent addition of more tracer. These multiple injections led to further complications in interpretation of results, thus it was determined that a single, larger injection of 5 g SF_6 was more appropriate.

3.1 Analytical Instruments

Prior to injections, the Laboratory collected and analyzed samples from borehole 54-24399 using data from both a field-deployed LumaSense Photoacoustic Gas Monitor INNOVA model number 1412i (hereafter, INNOVA, Figure 3.1-1) and Tedlar[®] sampling bags that were subsequently analyzed via OmniStar GSD 320 O Quadrupole Mass Spectrometry (hereafter QMS, Figure 3.1-2). These data were used to determine background SF_6 readings for both sampling methods (e.g., field and analytical laboratory). The Laboratory also collected background samples for SF_6 analysis from boreholes 54-01015 and 54-01016. Analysis showed that background for SF_6 at MDA L is below detection on both the INNOVA and QMS.

Figure 3.1-3 shows the INNOVA SF_6 calibration curve of INNOVA readout vs known concentration of SF_6 in LANL in-house reference tanks as well as zero air. In-house reference tanks span concentrations 0.1, 1, and 10 ppmv with uncertainty better than 1% specified value (within the bounds of the red symbols). Note that the INNOVA output is first order linear over four orders of magnitude including the range of measured values in this report ($R^2=0.9999$).

Figure 3.1-4 shows the QMS calibration curve with ion current vs known concentration of SF_6 in LANL in-house reference tanks as well as zero air. Note that QMS ion current is first order linear over four orders of magnitude ($R^2=0.9997$). As described in Section 4.3, the QMS data were heavily impacted by instrument temperature.



Figure 3.1-1 Innova 1412i Photoacoustic Gas Monitor, installed in the field at MDA L, April 2017.

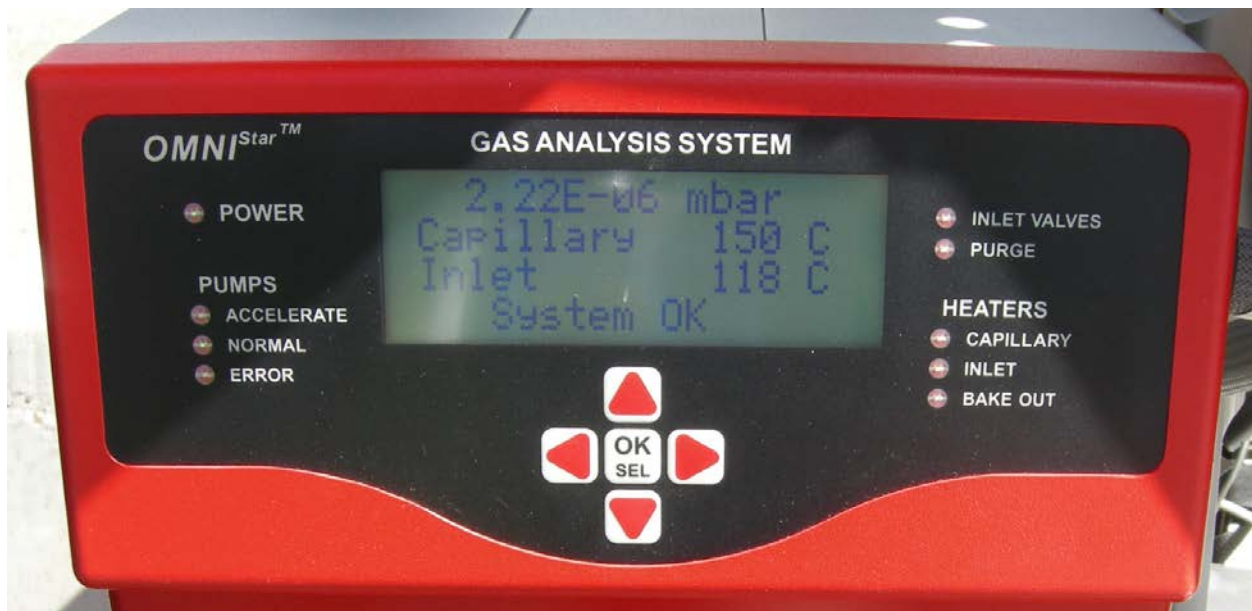


Figure 3.1-2 OmniStar™ Quadrapole Mass Spectrometer.

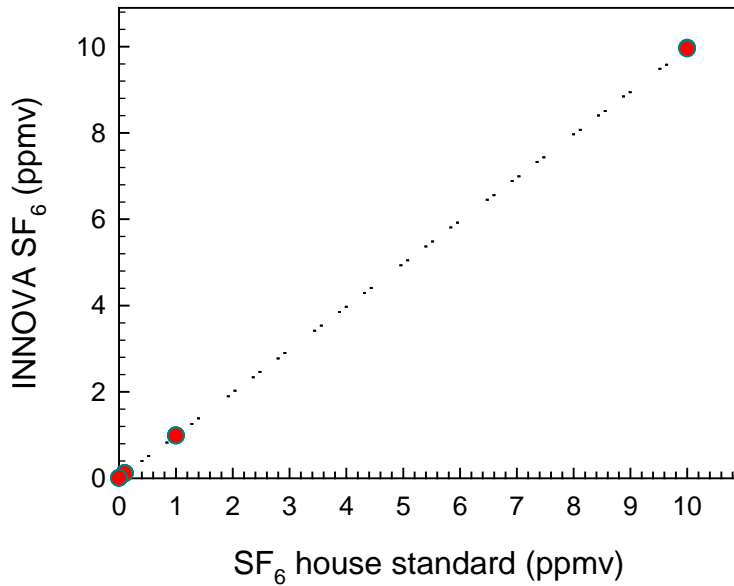


Figure 3.1-3 INNOVA calibration to LANL created SF₆ standards

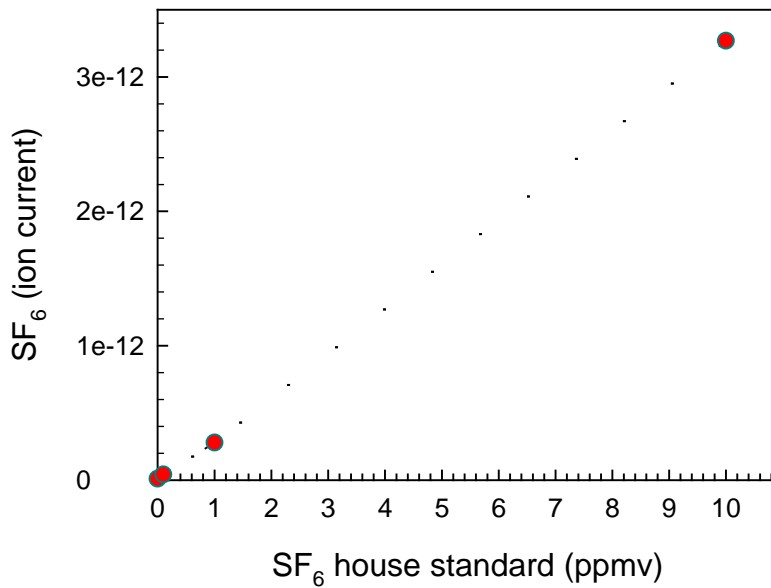


Figure 3.1-4 QMS calibration to LANL created SF₆ standards

3.2 Analytical and Field Methods

Gas phase measurements performed with the INNOVA are based on the fact that light energy absorbed by a gaseous molecular species is converted into pressure variations that can then be detected by sensitive microphones (REF). The energy absorbed, and hence the pressure variation measured, is gas

phase specific and a sequence of filters can therefore be employed to isolate and quantify the concentration of species of interest. The unit used in our tests was equipped with an infrared light source and a sequence of bandpass filters for SF₆, CO₂, tetrachloroethylene (PCE), trichloroethane (TCA), and H₂O. Instrument flow rate was approximately 2 liters per minute and response time was ~1 minute for the full suite of analytes. For the gas phase of interest, SF₆, the instrument detection limit was ~10 ppb. The instrument was factory calibrated immediately prior to field deployment and tested with in-house standards at 0.1, 1.0 and 10 ppm SF₆. Instrument response with in-house standards was linear over the range tested with accuracy of better than 1% of the measured value.

Additional gas phase measurements were performed with an OmniStar™ GSD 320 gas analyzer (Figure 3.1-2). The instrument is equipped with a Faraday detector for relatively high concentrations of gases and a more sensitive C-SEM detector for lower concentrations analysis. The detection limit of the Faraday detector is < 40 ppm and that of the C-SEM is < 1 ppm. The mass resolution of the instrument ranges from 0.5 to 2.5 mass unit at 10% peak height. The instrument is equipped with an inlet port connected to a 1 m long stainless steel heated capillary. Standard sampling volume is 0.65 mL/min; however this volume can be adjusted lower if needed. The instrument records ion current at the selected mass units. The ion current is converted to concentration using calibration curves established for select gases. It is important to note that the background ion current changes with temperature and therefore the calibration curves need to be established at the same temperature as the actual measurements. The unit was operated over the entire experiment with the exception of several periods of power loss. Ion currents were recorded for SF₆, Kr, Ne, CO₂, CO, and H₂O. The stainless steel sampling port was equipped with a needle and inserted into a Tygon tubing that sampled the top and bottom of the well. A solenoid valve operated by a data logger was programmed to alternate sampling between the two intervals. A calibration curve was established using gas standards with 0.1, 1.0 and 10 ppm SF₆ and used to convert ion current series to SF₆ concentrations.

To preempt pumping difficulties with the inboard INNOVA pump system in the field, air from the sampling zone was pumped to the surface with a supplemental diaphragm pump (Gast model number 10D1125-101-1052) that delivered a controlled flow of 2 liters per minute to a 10 liter buffer volume carboy (Figure 3.2-1). The buffer volume was required to eliminate large pressure swings at the inlet of the INNOVA when the internal pump would cycle thus eliminating automated pressure errors in the instrument software. During the test exercise in December of 2016, excess flow from the carboy was recirculated to the sampling zone below the packer. During the April 2017 experiment, excess flow from the carboy was released to the atmosphere. Further, to protect the equipment during the field testing, the equipment tower was protected by a tarp as shown in Figure 3.2-2. Sampling lines for both instruments were passed through desiccators filled with Drierite® (calcium sulfate) immediately after the wellhead sampling ports to prevent condensation of liquid water in the sampling lines and to reduce potential for interference during measurements. Desiccant was changed after visually confirming a color change from blue to light pink in approximately 50% of the desiccator chamber (upper left of Figure 3.2-3). Also shown on Figure 3.2-3 are sections of heat tape and thermal blankets used to warm the wellhead and further reduce issues with condensation and freezing.



Figure 3.2-1 10-L Carboy used as a gas reservoir to ensure continuous INNOVA operation.



Figure 3.2-2 Field equipment tower.



Figure 3.2-3 Wellhead with sampling lines connected to desiccant

3.3 Noble Gas Tracer

An attempt was made during April of 2017 to also include Krypton and Neon tracers. These tracers were successfully injected into borehole 54-24399. However, thermal impacts on the noble gas sampler (QMS) preclude the use of these data in the analysis. Temperature variation between day and night led to large swings in instrument response that cannot be easily corrected from the data. This was a valuable lesson learned, especially because the manufacturer assured the LANL team that the QMS would have no thermal effects in the field.

3.4 Pressure and Temperature Measurements

Pressure was recorded at the surface and in the tracer sampling zone of borehole 54-24399 at the base of the packer with Omega absolute pressure gauges (part #s PX409-015AI-EH [6 ft. 4-wire cable termination] and PX429-015AI-EH [milspec twist lock termination], respectively, 0.08% accuracy). Transducers were scanned every second and averaged over 6 minute intervals. Transducer excitation and logging of pressure data were performed with a Campbell Scientific data logger (model number CR5000, Figure 3.4-1). Temperature logs were downloaded from LANL's observational weather tower at TA-54 and also collected from the internal INNOVA temperature sensor.

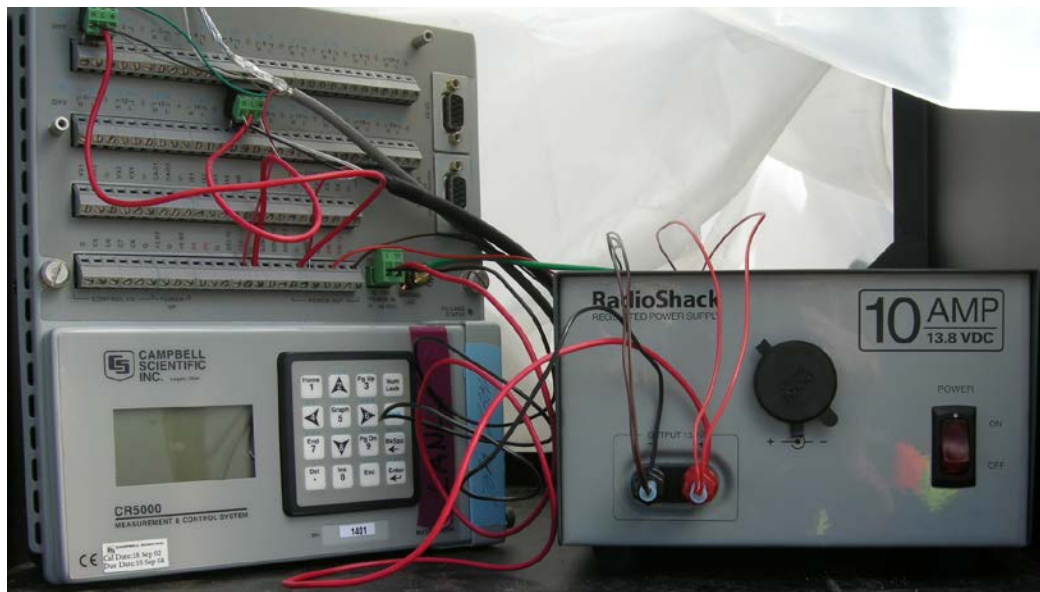


Figure 3.4-1 Campbell Scientific Data Logger CR5000 and 10 amp power supply.

3.5 Preliminary Test in December of 2016

A preliminary tracer test was performed in December 2016 to assess the workflow. Due to complexities including frozen sampling lines and low tracer recovery, data from this event are not discussed in detail. Results from this test were however very useful in planning the subsequent sampling in the spring of 2017. Briefly, results of surface pressure and SF₆ concentration at depth from the December 2016 test are shown in Figures Figure 3.5-1 and Figure 3.5-2. This testing period was elucidating in terms of understanding movement of tracer within the sampling zone below the packer. For instance, in the initial test, tracer was injected immediately below the packer at 566.7' bgs and the sample stream was pulled from 21 feet below the packer. Because in this initial test we chose to recycle air from the intake at the well through the analytical system and then back downhole, there was an initial pulse of tracer detected following injection due to residual tracer in the sampling loop but concentration quickly returned to background and was not observed again during the initial 24 hours of sampling. In late morning of December 13th, 2016, it was decided to switch the intake and return lines to see if tracer was observable at the depth at which it was previously injected and indeed, as highlighted in Figure 3.5-2, there is an immediate order of magnitude increase in SF₆ concentration (blue dots). This was the first observation that horizontal (cross-hole) flow was the dominant driver of tracer dispersion and that vertical diffusion or gravitational flow might be secondary. The INNOVA intake remained on this port for the rest of the experiment through December 15, 2016.

On December 14th, 2016 at 2:30 AM, concentrations of SF₆ in the INNOVA jumped rapidly. This rise in concentration is not associated with any injection or switching of the sampling ports. The sudden rise in concentration mimics behavior seen in the pre-test numerical modeling (Figure 2.2-2) and provides additional evidence for lateral shifting of a discrete plume as barometric pressure drags the initial injected mass back and forth across the monitoring location. A smaller but still significant jump in concentration occurred again on December 14th at 7:00 PM. The dynamic nature of the plume behavior encouraged development of a second tracer test with tighter controls on injection. The goal of the second test, undertaken in April 2017, was to develop a data set that could be used to more definitively

constrain gas migration in the Cerros del Rio basalts.

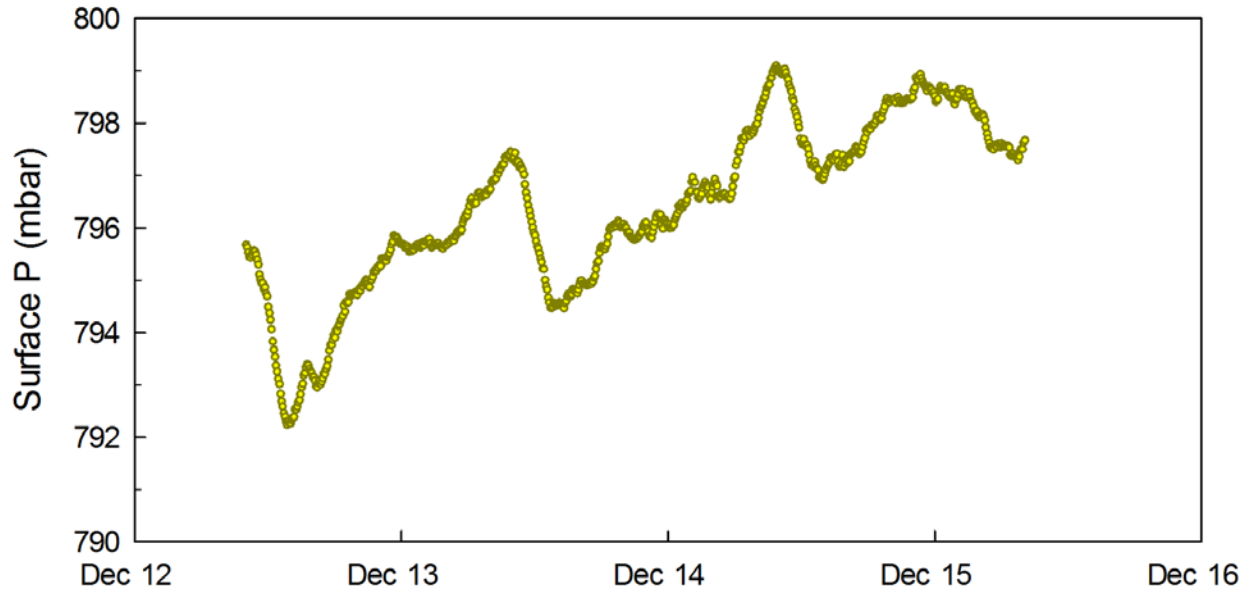


Figure 3.5-1 Pressure during the Dec. 2016 preliminary tracer test

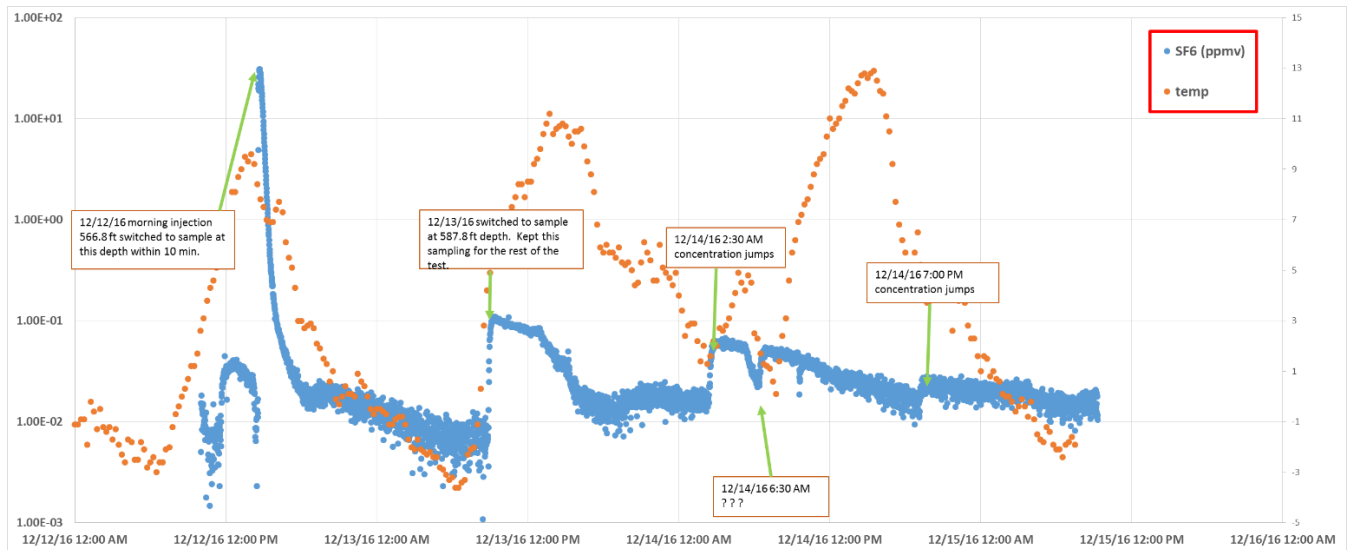


Figure 3.5-2 Timing of SF₆ injections, measured SF₆, and temperature during the Dec. 2016 preliminary tracer test

3.6 April 2017 Tracer Tests

3.6.1 Injection and Sampling at 566.7 ft bgs

Starting at 2:48 PM on April 5, 2017, tracer was injected into borehole 54-24399 via a dual-port packer system (Figure 1.2-5). A 1 L Tedlar® bag (5 g aliquot) of the tracer SF₆ was injected in the open borehole through the injection/return flow tubing shown schematically in Figure 3.6-1. This injection was made via a large volume syringe into a ‘T’ immediately downstream of the downhole flow pump to insure that all tracer was ultimately delivered to the port open to the basalt below the packer at 566.7 ft bgs.

Immediately after the injection of the SF₆ (2:52 PM) a similar 1 L Tedlar® bag of neon was injected to the port at 566.7 ft bgs. Flow of ~2 liters per minute to the packer outlet was continued for 10 minutes to ensure that the entire volume of tracer was flushed through the downhole tubing (~2.17 L in volume, assuming an inner tubing diameter of 4 mm for the ¼" OD tubing). After injection and flushing of the tubing to 566.7 ft bgs, the pump was reversed and sampling was initiated with the INNOVA from the 566.7' BGS at 3:08 PM. INNOVA data were recorded approximately every 57 seconds.

3.6.2 Injection and Sampling at 587.8 ft bgs

Beginning at 3:04 PM on April 12, 2017, a 1 L bag of krypton was injected to the port at 587.8 ft bgs following the same procedure used for the injections at 566.7 ft bgs. At 3:07 PM the injection of krypton was completed and followed by purge of fresh air until 3:26 PM when the sample line was reconnected to the QMS. The sampling line for the QMS was pulled from depth via a Gast diaphragm pump (model # 10D1125-101-1052, 12VDC) with flow through a needle valve to control flow rate to 50 milliliters per minute (mLpm). The QMS subsampled this flow at a rate <1 mLpm and the excess was exhausted to the atmosphere. The QMS scanned a specified mass range (4 to 150 AMU) continuously with results being recorded every ~12 s.

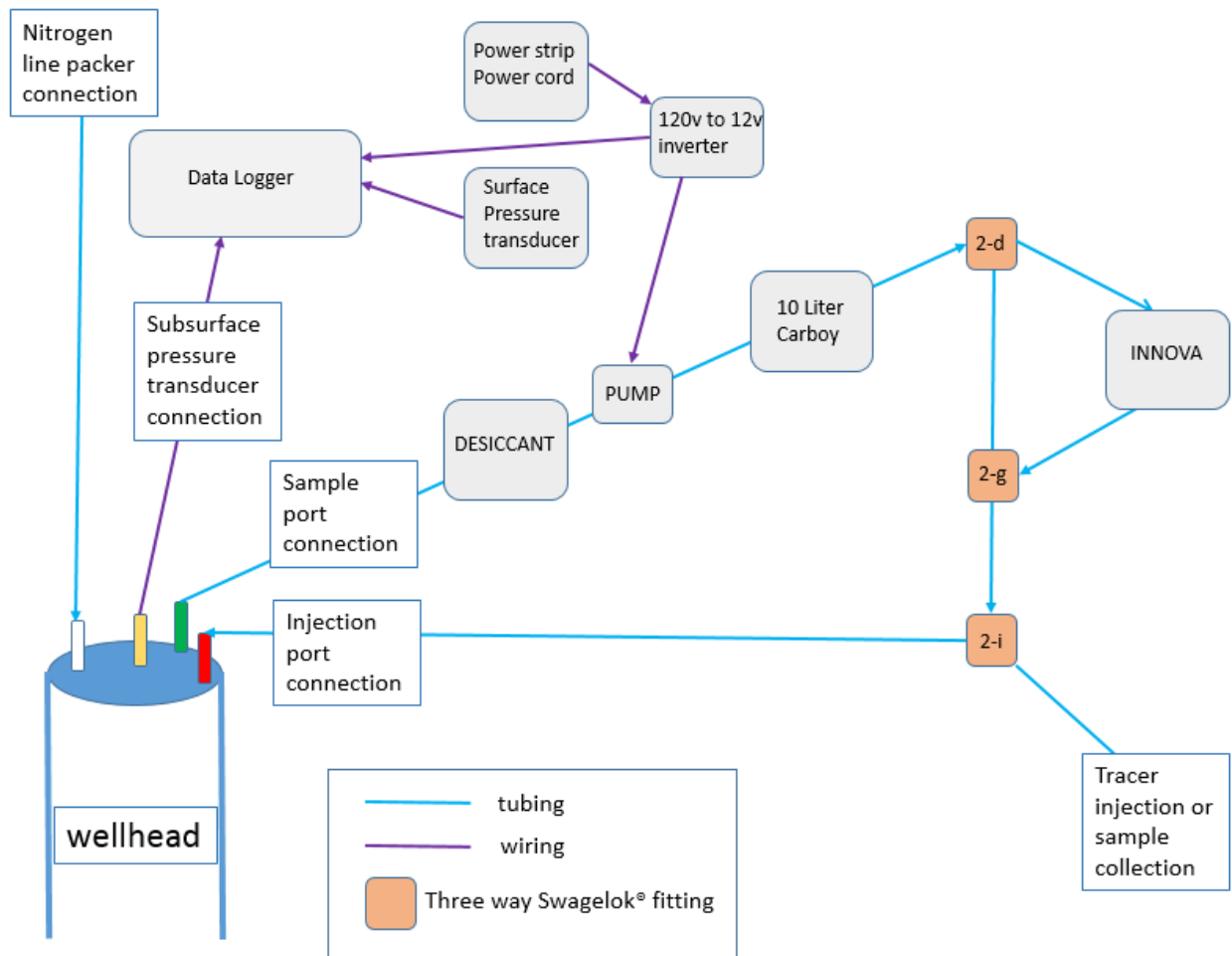


Figure 3.6-1 Schematic of sampling train at the surface of borehole 54-24399.

3.7 Sampling at Secondary Wells

Sampling was also performed at ports in boreholes 54-01015 and 54-01016 to validate model performance and provide additional data to better quantify the influence of the barometric pumping effect on tracer transport. These two angled boreholes have ports in the basalt approximately 30–76 m (100–250 ft) laterally from borehole 54-24399 and are the only nearby boreholes that penetrate the basalt with dedicated sampling ports. Neither of these two wells penetrate as deep into the basalt as 54-24399 (Neeper 2002). Sampling at these boreholes was performed by grab sampling with Tedlar® bags and analyzed by QMS in the laboratory. During April of 2017, no detects of SF₆ were seen in either well 54-01015 or 54-01016.

4 Results from the April 2017 Tracer Test

4.1 Pressure Results

Pressure data were recorded prior to and during the tracer injection test between the dates of Monday, April 3 and Monday, April 17, 2017. During this period, surface pressure varied between 784 and 800 mbar absolute pressure (Figure 4.1-1). Daily cycling of pressure with midday highs and nighttime lows having an amplitude of 3 to 5 mbar was overlain by low and high pressure periods driven by synoptic scale weather patterns. These longer period oscillations lasted one to several days and imposed an amplitude of 10 to 15 mbar on the surface pressure signal. Data recorded at depth revealed similar patterns but with less high frequency variation and a lower amplitude in the diel variation of 2 to 3 mbar. The amplitude of synoptic forcing was more similar to the amplitude observed at the surface. These details can be observed in Figure 4.1-2 where surface pressure has been altitude adjusted by 567 feet for comparison to downhole pressure. Another pattern to note when comparing surface vs. downhole pressure in Figure 4.1-2 is the time lag of the downhole pressure relative to the atmospheric forcing. This lag is typically on the order of 2 to 3 hours. The result is an altitude adjusted difference of atmospheric to downhole pressure that varies from positive ~6 mbars to -4 mbars (Figure 4.1-3).

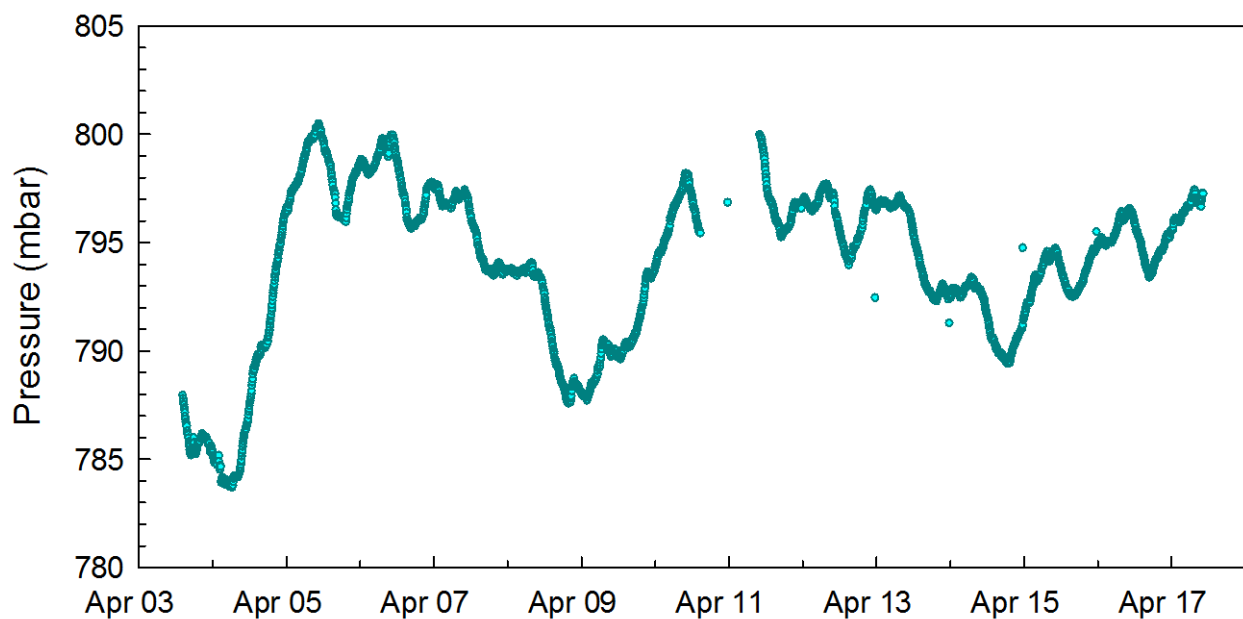


Figure 4.1-1 Measured surface pressure at MDA L, April 3-17, 2017.

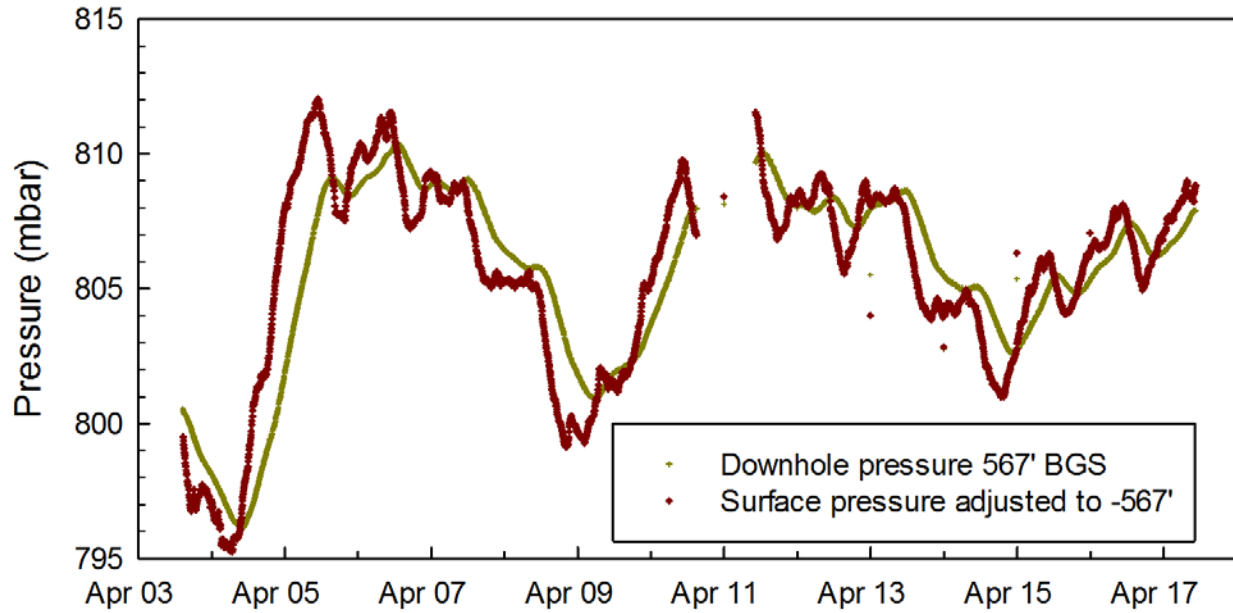


Figure 4.1-2 Measured surface pressure adjusted to the same mean value as measured downhole pressure at 566.7 ft bgs.

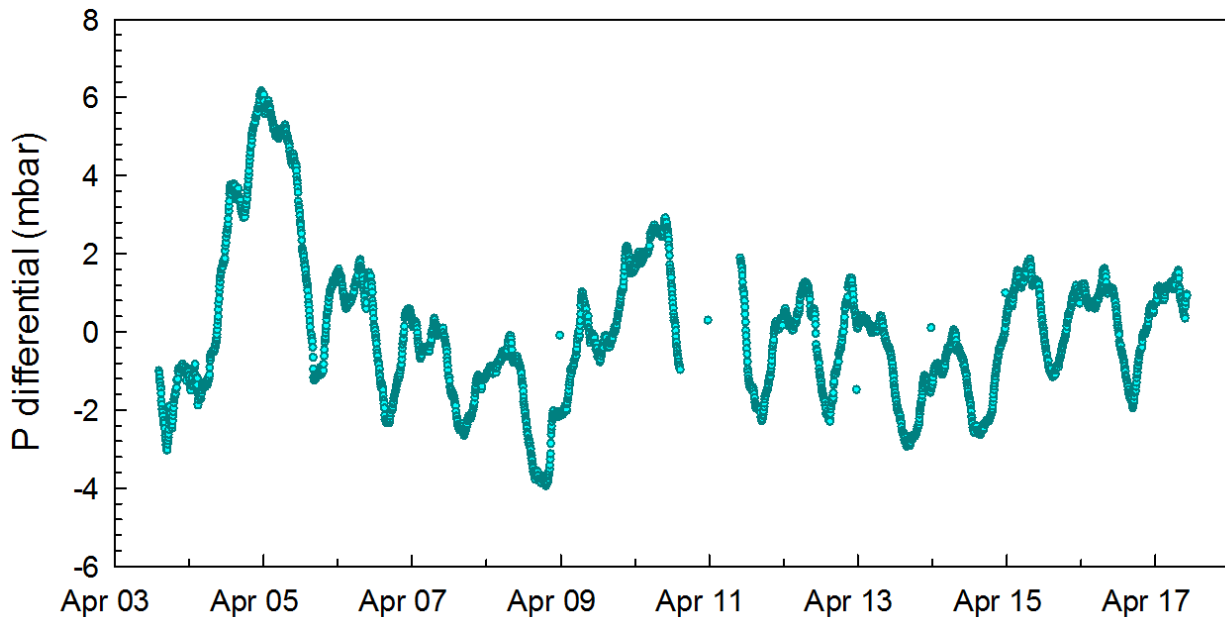


Figure 4.1-3 Measured pressure differential between surface and downhole (566.7 ft bgs) for April 3-17, 2017.

4.2 INNOVA Results

4.2.1 Data Gaps

During the course of the tracer tests, there were several periods where the sampling system integrity was compromised. These periods were the result of a variety of causes (e.g. periods where power to the pumps was lost, times when the system plumbing had to be opened in order replace desiccant, etc.).

These periods hold the potential to yield erroneous results from the INNOVA that could result in misinterpretation of tracer data. Observation of CO₂ (Figure 4.2-1), which is produced at depth by microbial respiration, allows us to filter data that might be compromised. Any time that CO₂ concentration approaches atmospheric background values, we consider SF₆ likewise has been diluted and is therefore not a reliable measurement of the true downhole concentration. All INNOVA data with CO₂ concentration less than 800 ppm are considered suspect and are therefore not utilized in our analysis.

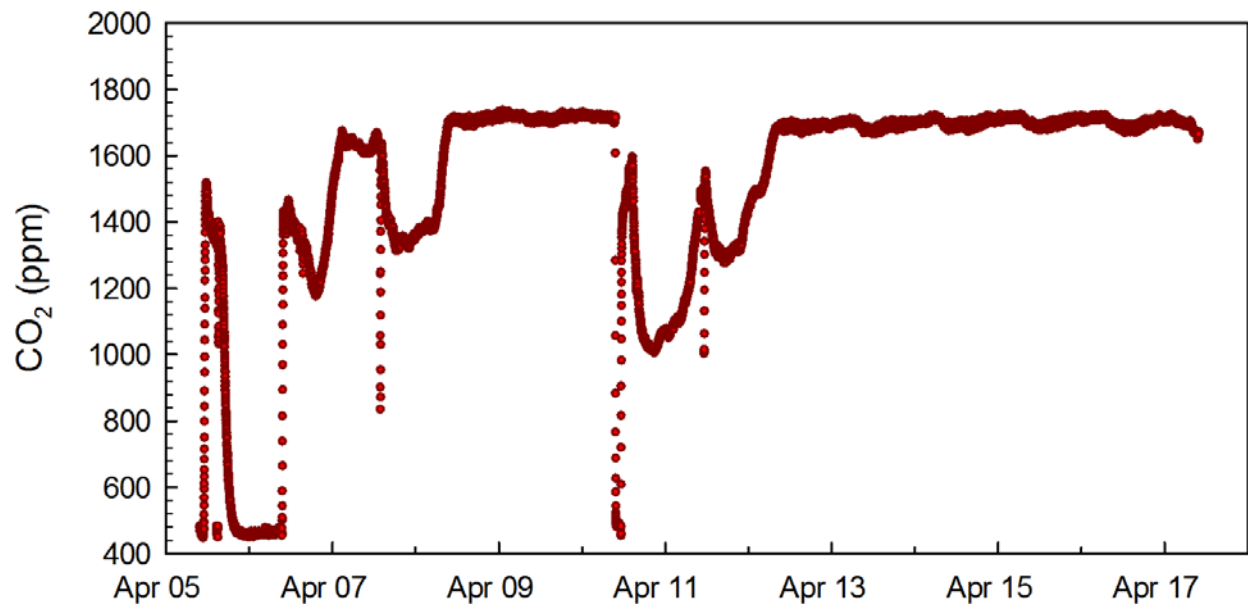


Figure 4.2-1 Subsurface CO₂ as an indicator of data quality

4.2.2 Sulfur Hexafluoride Results

SF₆ concentrations from the borehole after CO₂ filtering are shown in Figure 4.2-2 as a six minute running average. The early part of the record is off linear scale so an inset figure at log scale is presented. An initial drop from 150 ppmv (150,000 ppbv) to 0.01 ppmv (10 ppbv) is followed by a recovery to concentrations of several hundred ppbv before concentrations appear to level off at between 20 and 50 ppbv. The character of the tracer evolution compares well with the pre-test prediction for barometrically pumped tracer behavior shown in Figure 2.2-2. The character of the measured tracer response is not similar to the pure diffusion calculation shown on Figure 2.2-2, implying that calculations for transport across the Cerros del Rio basalts toward the regional aquifer should re-evaluate the use of simple diffusive transport models such as in Tier II screening (LANL 2011).

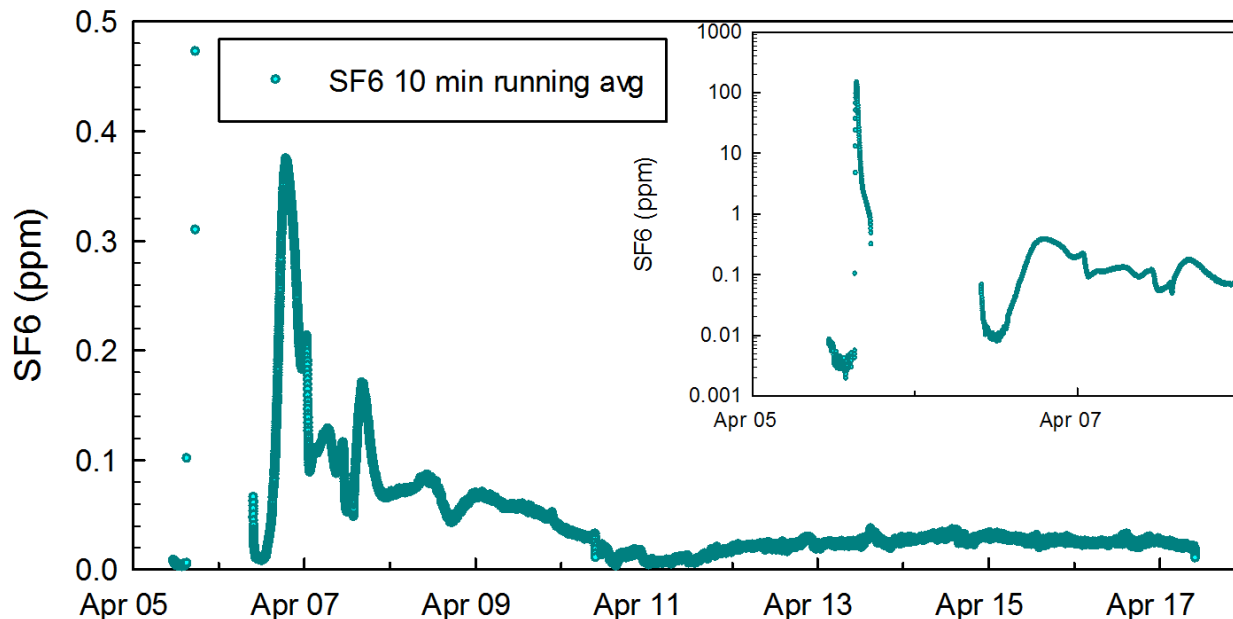


Figure 4.2-2 SF₆ data collected with the INNOVA from April 5 – 17, 2017.

4.2.3 1,1,1-TCA and PCE Results

Although not part of the tracer test as defined, it is also interesting to note that the INNOVA also measured variability in PCE and 1,1,1-TCA concentration in the open, uncased section of the borehole that were strongly correlated with pressure variations.

Figure 4.2-3 shows 1,1,1-TCA data collected during the sulfur hexafluoride (SF₆) tracer test performed in April 2017. Included in Figure 4.2-3 is the subsurface pressure signal beneath the packer during the experiment. These data show 1,1,1-TCA concentrations varying by nearly 2 orders of magnitude, closely tied to changes in subsurface pressure. Figure 4.2-4 shows 1,1,1-TCA plotted with surface temperature, indicating little dependence of the INNOVA TCA measurements on temperature. Blue vertical lines on this and the next two figures are guides to show the correlation between temperature and concentration.

Both PCE and temperature are plotted in Figure 4.2-5. From April 5 until the evening of April 8, PCE rises from near 50 ppbv to over 200 ppbv followed by a similar decrease from April 8 through April 11. Beginning on April 12, PCE concentration begins to track temperature closely and these data are suspect. Light blue guide lines on Figure 4.2-5 highlight the apparent temperature impact on the INNOVA measurements beginning April 12. However the data prior to April 12 for PCE do not show correlation to temperature and support the TCA data showing evidence for discrete, higher concentration regions of contamination moving through the basalt.

Given the behavior of TCA and PCE seen during the tracer experiment, our conceptual model for transport in the deep basalt continues to evolve.

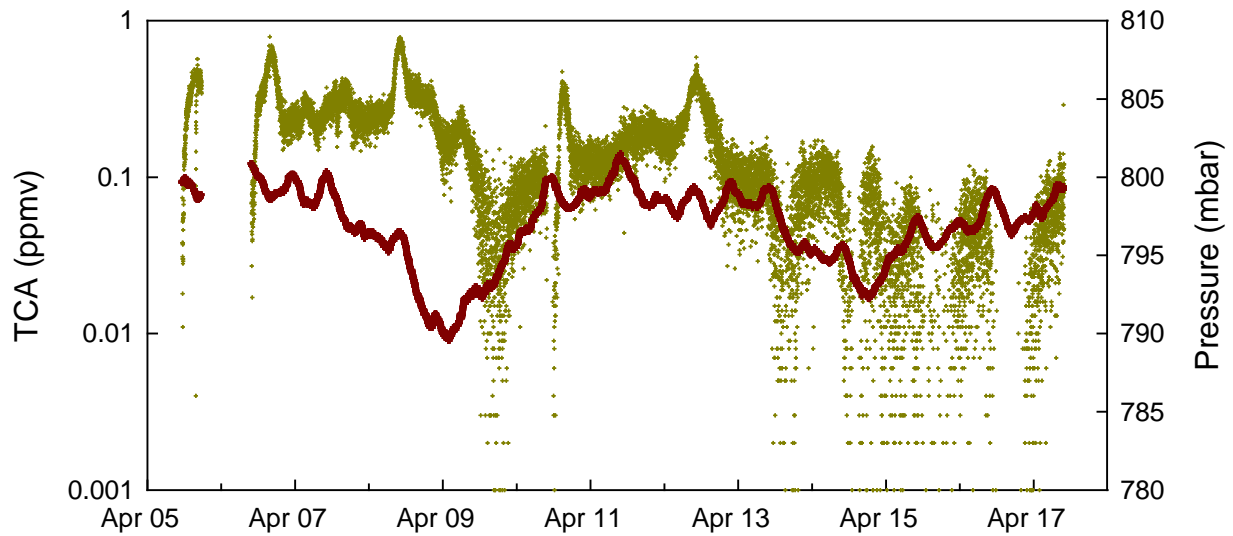


Figure 4.2-3 INNOVA measures (gold) of 1,1,1-TCA concentration from borehole 54-24399 during 12 days in April 2017. Pressure measured beneath the packer is also shown (red).

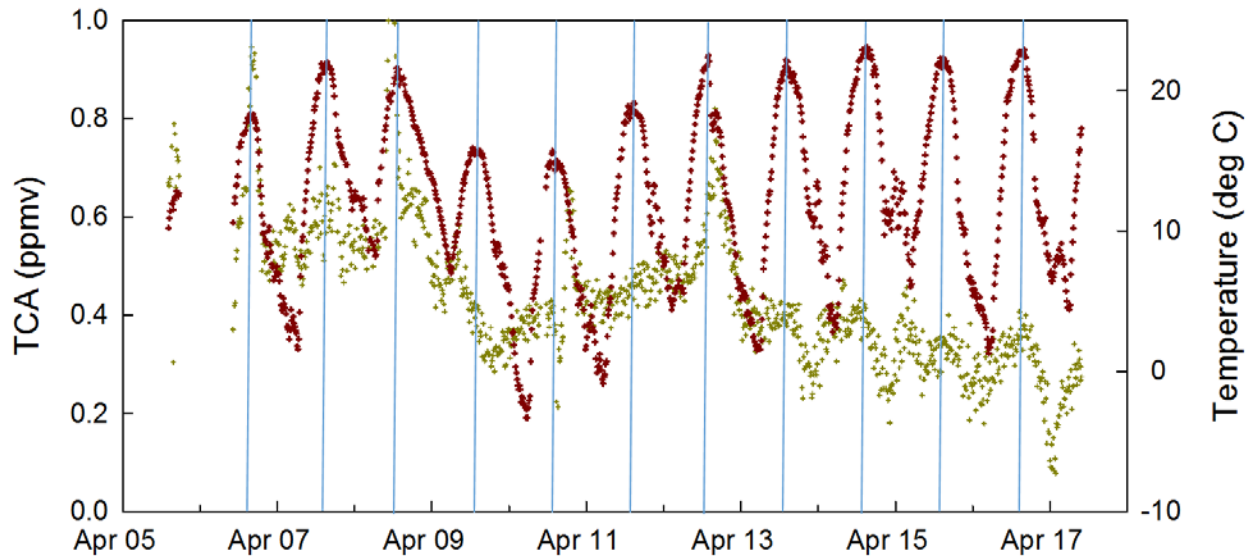


Figure 4.2-4 INNOVA measures (gold) of 1,1,1-TCA concentration from borehole 54-24399 during 12 days in April 2017. Measured surface temperature is also shown (red).

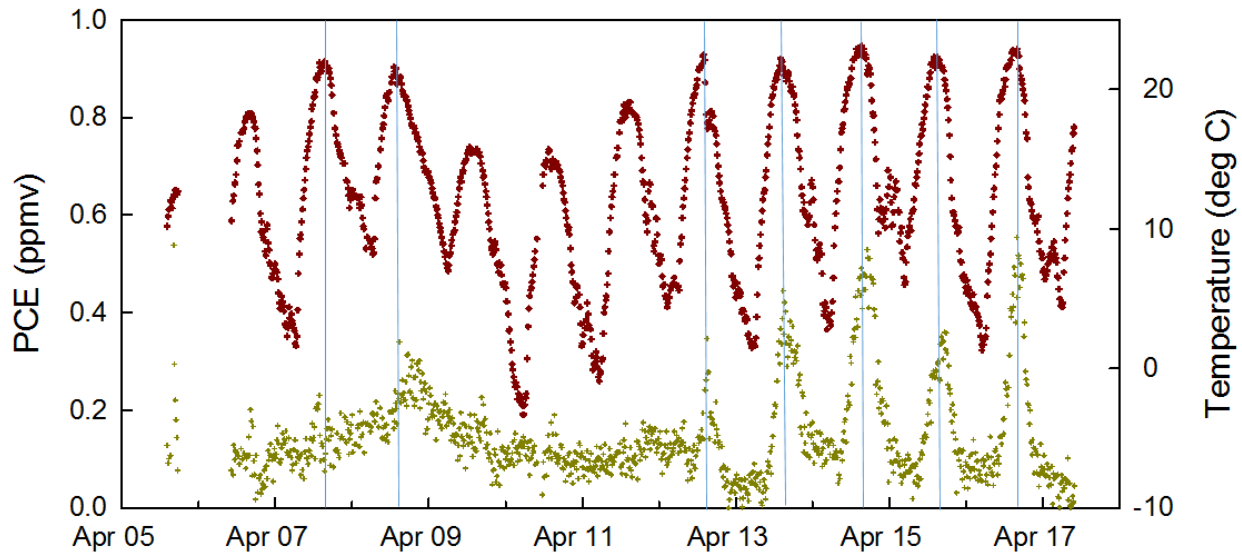


Figure 4.2-5 INNOVA measures of PCE (gold) from borehole 54-24399 during 12 days in April 2017. Measured surface temperature is also shown (red).

4.3 QMS results

QMS results are displayed in Figure 4.3-1. It is readily observed that recorded concentrations for SF_6 (green symbols) are as high as 2 ppm after the initial drop-off after injection and that concentrations of this magnitude are a factor of 5 or more greater than those recorded by the INNOVA. It is also apparent that these daytime spikes in recorded concentration are highly correlated with daytime high temperatures (red symbols in Figure 4.3-1). Other data from the QMS that are not shown exhibit similar dependence of instrument response to ambient temperature changes. We conclude that this first attempt to deploy the QMS for field operations was unsuccessful but that while this is disappointing and excludes comparison of results from two depths in the borehole, instrument sensitivity is good and with proper control of instrument conditions, the QMS should be a useful tool for future operations.

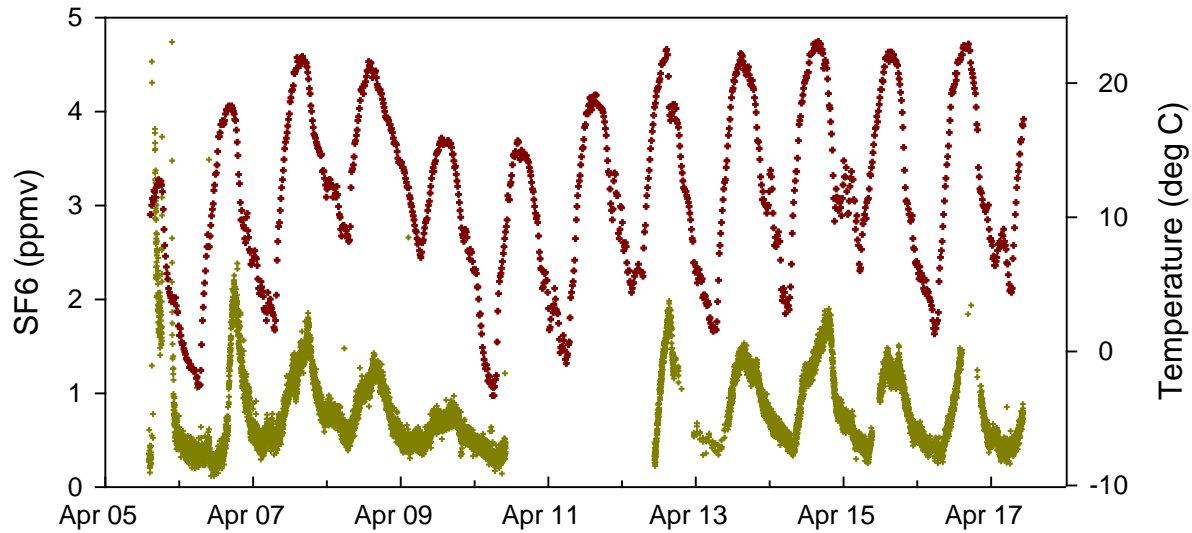


Figure 4.3-1 SF₆ (gold) and surface temperature (red) versus time for the QMS.

5 Post-Test Analytical Analysis and Scoping Calculations

The dimensions of the domain in the present problem are largely unknown. As Neeper's work notes (Neeper 2002 and 2003), a potential basalt venting location is present as a hole in an outcrop approximately 3.8 km southeast of the site. However, the basalt may also be ventilated at many locations, including in areas between 1 and 3 km to the east/southeast of the site where only a thin soil layer remains on top of the basalt. The following work presents our efforts to address this uncertainty and determine the scale and configuration of the domain used for numerical simulations of transport.

5.1 Analytical Analysis

We first characterize the porous media by comparing the atmospheric and downhole pressure signals in terms of signal attenuation and time lag. In keeping with the methods of Neeper (2002), the atmospheric and subsurface pressure data were transformed to a Fourier series for the 12 days over which the experiment took place. The quantities of interest are the amplitude ratio A_r and phase shift ϕ_s measured at the well sensor for any particular period, T_n :

$$A_r = \frac{P_n(x)}{P_{n0}(x=0)},$$

$$\phi_s = \varphi_n(x) - \varphi_n(x=0),$$

where x is the distance from the atmospheric boundary to the well sensor. The resulting spectral density allows us to choose a dominant period of 1.1 days and associated barometric pressure amplitude of 46.3 Pa to drive our model (Figure 5.1-1).

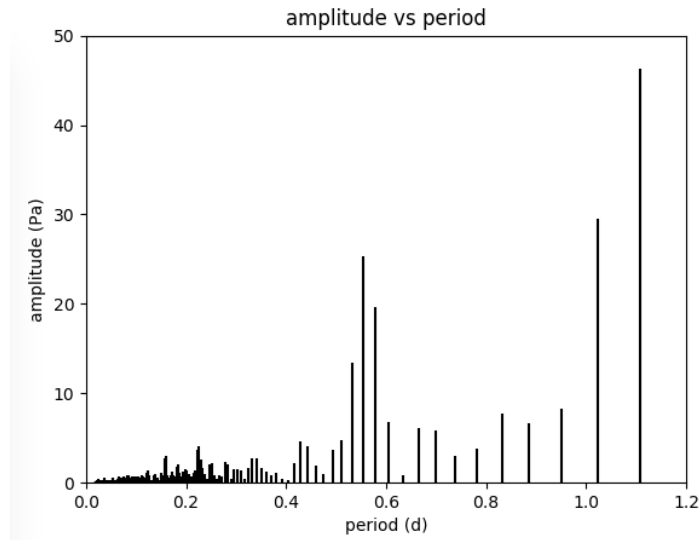


Figure 5.1-1 Spectral density

The associated amplitude ratio and phase shift are included as parameters in the analytical solution to isothermal flow of an ideal gas through a homogeneous porous medium with harmonically varying surface pressure in work by Nilson et al. (1991, eqn. 3):

$$\frac{p - p_0}{\Delta p} = \frac{\cosh \lambda \sqrt{i} \left(1 - \frac{x}{L}\right)}{\cosh \lambda \sqrt{i}} e^{i\omega t}$$

where $\sqrt{i} = (1 + i)/\sqrt{2}$ and

$$\lambda = L \sqrt{\frac{\omega}{\alpha}} = \left[\frac{2\pi}{\alpha T / L^2} \right]^{1/2}$$

We make the adjustment that, rather than depth, x represents horizontal distance from the atmospheric outcrop to the monitoring well through the porous medium. In so doing, this solution is analogous to Neeper’s (2002, eqn. 4) “finite-depth” model (Figure 5.1-2).



Figure 5.1-2 Schematic of the domain. Distance from wellbore to atmosphere is x.

Using the $k = 7.7 \times 10^{-9} \text{ m}^2$ and porosity 0.35 derived by Neeper (2002), we designed an optimization problem in order to solve for our domain length, L , and well distance, x . We define a combined residual for our measured amplitude ratio and phase shift for the period $T = 1.1$ days when compared to the simulated values. We then find the global minimum for the residual using a stochastic population based algorithm that samples the candidate space (Storn and Price, 1997). For robustness, we designated the candidate space to have a wider range of values for the domain than we expect possible given our spatial and geological constraints; the algorithm's initial population of "guesses" was performed via Latin Hypercube sampling within the ranges

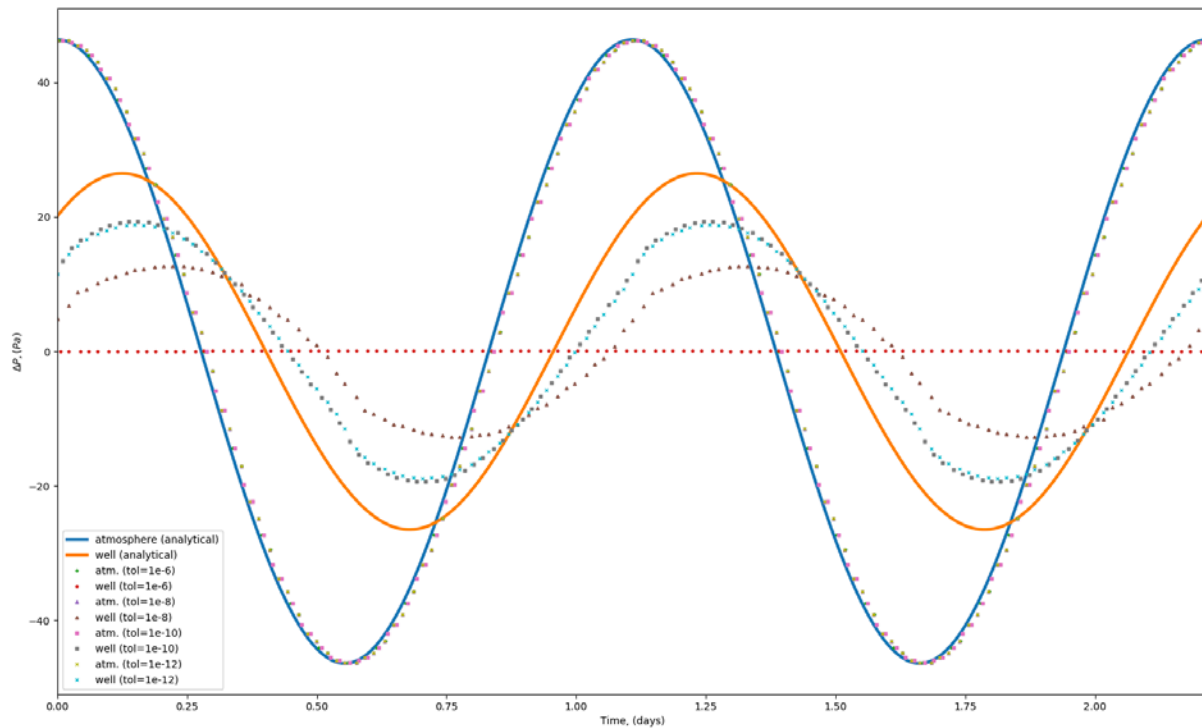
$$250 \text{ m} \leq L \leq 4000 \text{ m},$$

$$10 \text{ m} \leq x \leq 3990 \text{ m}$$

This method yielded the optimized domain parameters $L \sim 2450 \text{ m}$ and $x \sim 900 \text{ m}$. The overall length of the domain agrees closely with that of Neeper ($L = 2500 \text{ m}$), however, using the data from borehole 54-24399, the well is located approximately 500 m closer to the atmospheric opening and a congruent distance farther from the closed boundary than that calculated by Neeper (2002). It should be noted that the work done by Neeper (2002) took place at a different set of wells than in the present work. We used these optimized spatial parameters to inform our numerical modeling efforts.

5.2 Scoping Calculations

Our initial FEHM numerical simulations produced overly attenuated downhole pressure responses, to the point that the pressure propagation front was nearly imperceptible at the tracer injection site; so damped was the signal that essentially no transport took place. It was found that the FEHM solution was highly sensitive to the global tolerance of the linear equation solver, which is comprised of product of the machine tolerance and the Newton Raphson residual tolerance. To determine the optimal global tolerance to minimize numerical damping, we compared the analytical solution for downhole signal response with harmonically varying pressures (Eqns. 5,6; Nilson et al., 1991) to an analogous conceptual model in FEHM. We used a signal period $T = 1.1$ days with surface pressure amplitude of 46.31 Pa to drive the simulations. As evident in Figure 5.2-1, reducing the global tolerance likewise reduces the amount of numerical damping. For example, tightening tolerance from 10^{-8} to 10^{-10} reduced numerical damping from 52% to 27%. Further tightening global tolerance to 10^{-12} did not noticeably improve the simulation.



S-2.

Figure 5.2-1 FEHM pressure responses with varying global tolerances compared to the analytical solution.

The numerical damping is likely a function of the pressure signal frequency such that higher frequency signals experience more numerical dampening in numerical simulations. To test this, we ran an otherwise identical FEHM simulation in which we changed the period of the atmospheric pressure signal, increasing it from 1.1 to 7.305 days (Table 5.2-1). This isolates the effect of frequency on the numerical simulations, despite the improbability that a 1-day and 1-week signal would have the same amplitude. Using a global tolerance of 10^{-10} , we found the numerical damping for $T = 7.305$ days to be only 4%, confirming our hypothesis that the numerical simulations have difficulty effectively transmitting pressures at higher frequencies. Note that the results in the table for $T = 1.1083$ days are those presented in Figure 5.2-1. The results for $T = 7.305$ days show the reduction of numerical damping in the numerical simulations when the signal frequency is lower. This is important to note for pressure propagation simulations with larger spatial domains, wherein one or both of the tolerances comprising the global tolerance are often loosened to reduce computational expense. Care should be taken to ensure that the global tolerance employed is numerically as well as computationally appropriate for the problem domain.

Table 5.2-1 Numerical damping and global tolerance sensitivity analysis results.

<u>T = 1.1083 days</u>	Analytical Solution	FEHM (global tolerance)		
		<u>10⁻⁶</u>	<u>10⁻⁸</u>	<u>10⁻¹⁰</u>
Barometric amplitude (Pa)	46.311	–	–	–
Downhole amplitude (Pa)	26.477	0.059	12.745	19.381
% Numerical Damping	–	99.8%	51.9%	26.8%
<u>T = 7.305 days</u>				
Barometric amplitude (Pa)	46.311	–	–	–
Downhole amplitude (Pa)	44.750			42.94
% Numerical Damping	–			4.0%

6 Post-Test Numerical Modeling

Data collected during the tracer experiment are next used to create a numerical representation of the experiment. The resulting simulations of both pressure variation and tracer migration and dilution are used to explore our conceptual model of this system. Further, the tracer test data can help to constrain aspects of the physical system such as permeability, porosity, and dispersivity. Previous reports and journal publications on simulations of the MDA L organic vapor plume can be found in Stauffer et al. (2005, 2007, and 2011) and LANL (2011 and 2014).

6.1 Model Domain

The 3-D geometry of the simulated system consists of an interval spanning the distance from the bottom of the deeper sampling port to 2 m above the upper sampling port. The domain is 8 m in the vertical direction and 20 m wide, with the borehole and sampling ports centered (Figure 6.1-1). The domain is divided into two rock types, massive basalt with very low porosity and rubblized basalt with high porosity. The mesh includes a high resolution borehole using the wellbore macro within FEHM, with a central radius of 0.07 m (.22 ft). The upper and lower sampling/injection ports are shown in Figure 6.1-1. The borehole runs the entire 8 m vertical length of the domain, with the upper 3.5 m of the borehole sealed off and set to impermeable and non-diffusive. Porosity in the open section of the borehole is set to 0.999, while permeability in this section is fixed at 10^{-4} m^2 based on previous modeling (Stauffer et al., 2007)

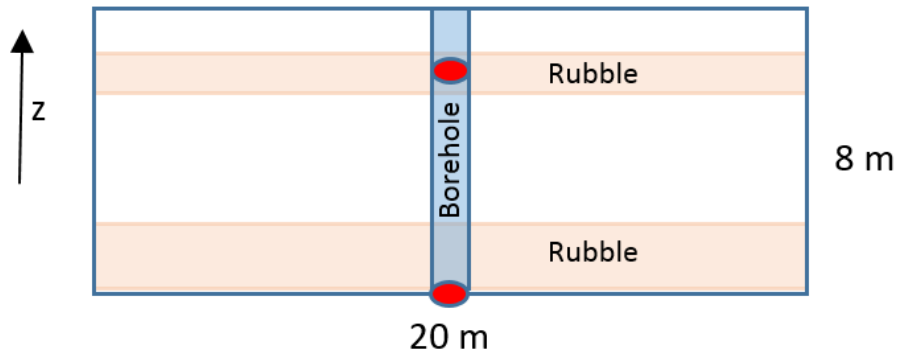


Figure 6.1-1 Model domain schematic, X-Z plane. Sampling ports are shown in red.

The third dimension of the mesh extends from 0 - 2500 m, with borehole 54-24399 located at 1100 m (Figure 6.1-2). The 2500 m mesh allowed the boundaries to be adjusted such that the measured atmospheric forcing could be moved to the point at which the measured pressure response beneath the packer was recreated in the simulations. Mesh spacing is 1 m in all directions within 100 m on either side of the borehole. Past this central higher resolution section, mesh spacing increases geometrically to a maximum Y spacing of approximately 10 m. Spacing in the X-Z plane remains 1 m throughout the mesh. In Figure 6.1-2, $Y = 0$ is on the right edge, while the wellbore shown in blue is located at $Y=1100$ m. The atmospheric boundary condition can be moved closer or further from the wellbore, to a maximum of distance of 1400 m at the far boundary where $Y=2500$ m.



Figure 6.1-2 Model domain schematic Y direction.

6.2 Material Properties

To explore the potential for barometrically induced spreading in the basalt, we have based our initial conceptual model on the work of Neeper (2002). In this work, a fit to pressure data from boreholes 54-01015 and 54-01016 were used to estimate properties of the subsurface, including permeability, porosity, and the distances to atmospheric outcrops. Neeper found that to match the pressure response between these two wells, a 1-D analytical model required an outcrop located on order of 1.5 km from the wells, and a relationship between porosity (ϕ) and permeability (k) such that

$$k/\phi = 2.2 \times 10^{-8}$$

Based on personal communications with Dave Broxton (LANL), the porosity of the rubblized basalt was assumed to be 35%, leading to an estimated $7.7 \times 10^{-9} \text{ m}^2$ permeability, or over 7000 darcies. For the massive basalt, where flow is primarily through fractures, we use the cubic law that relates aperture (a) to fracture permeability (k_f) as:

$$k_f = a^2/12$$

From this function, the bulk permeability of a porous medium can be estimated assuming a parallel fracture model with one fracture of aperture (a) per meter as:

$$k = a^3/12$$

For the simulations presented, an aperture of 4 mm was assumed, leading to a bulk permeability of the massive basalt of $5.3 \times 10^{-9} \text{ m}^2$ and a corresponding porosity of 0.004.

6.3 Boundary Conditions

Guidance from Neeper 2002 for the approximate distance to the far-field atmospheric boundary suggested that this boundary be located 1.5 km from borehole 54-24399. Subsequent analytical and numerical modeling done as part of this study (Section 5) place the atmospheric boundary closer to 1 km from borehole 54-24399. For the simulations presented, the atmospheric boundary is located 1 km from borehole 54-24399.

Using a global tolerance of 10^{-10} , and a maximum mass transfer time step of 0.052 days, the simulation is initialized with a 1 month pressure history from TA-54 adjusted to the correct elevation such that the mean of the weather station data are set equal to the mean of the data collected from the borehole transducer located beneath the packer (Figure 6.3-1). As shown, the atmospheric pressure driver used in FEHM exactly captures the measured data from the TA54 weather station.



Figure 6.3-1 Measured atmospheric pressure, March 5 – April 17 at TA-54, simulated atmospheric pressure boundary, and measured downhole pressure beneath the packer in borehole 54-24399 at 566.7 ft bgs.

The next test of the simulation is to compare the measured pressure response at 566.7 ft bgs to the simulated response. Figure 6.3-2 shows that the simulated pressure response at 566.7 ft bgs is quite similar to the measured data, giving confidence that the gas flow driven by the atmospheric boundary condition recreates conditions in the simulated subsurface.

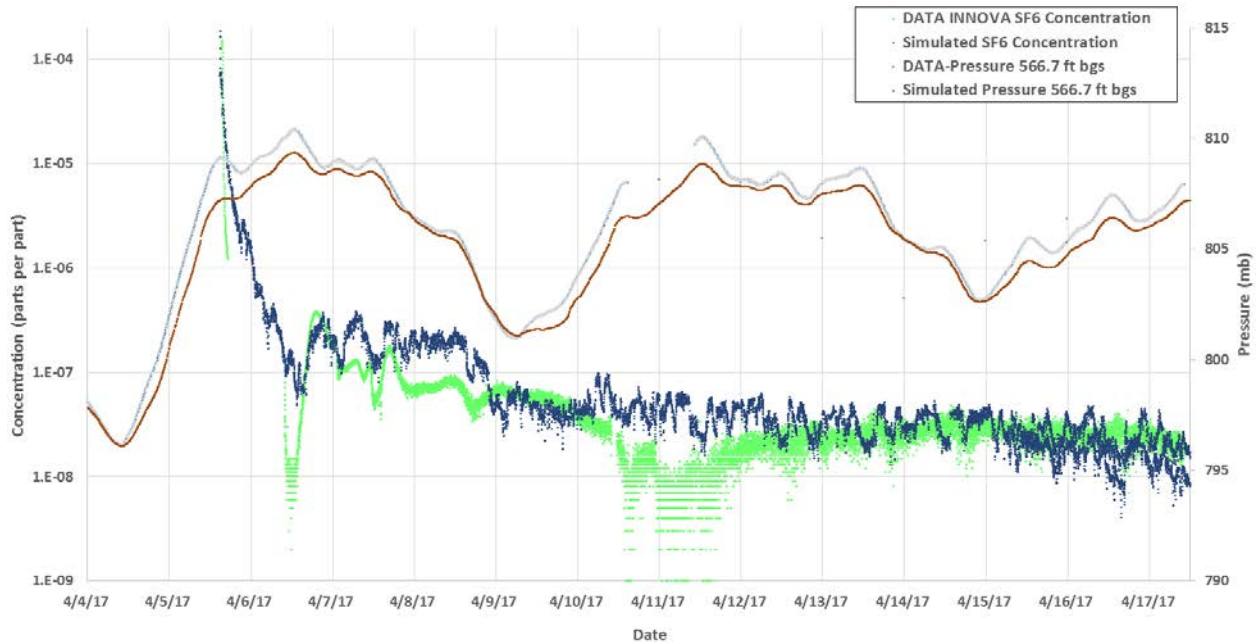


Figure 6.3-2 Data versus simulation results at 566.7 ft bgs for SF₆ concentration and pressure.

The best fit tracer response is also shown on Figure 6.3-2, where concentration is expressed in parts per part, such that 1e-6 is 1 ppmv and the detection limit of the INNOVA is on order of 1e-8. One major difference between the field data and the simulation is that the simulation required 90% of the injected mass to be removed from the measurement interval to achieve the fit between simulation and data seen in the figure. We hypothesize that mass was lost down the 90+ ft open borehole during the injection phase, leaving only a fraction of the injected SF₆ available for transport laterally through barometric pumping. SF₆ has a density that is 5x higher than air, and would tend to drop due to gravity until its concentration falls below approximately 0.1% by mass, or 200 ppmv (2e-4 on the figure, the highest simulated concentration shown). This hypothesis is supported by the fact that the highest measured concentration immediately after injection of 2 L/min for 10 minutes (tracer chaser) was 150 ppmv at 3:30 pm on April 5, 2017.

6.4 Estimating in situ Dispersivity

One goal of the simulations is to estimate an effective diffusivity for the basalt based on mechanical spreading induced during barometric pressure changes. In the absence of a velocity field, spreading is caused by simple molecular diffusion. Addition of a velocity field results in hydrodynamic dispersion, where spreading is related to molecules taking different pathways through a porous media. As gas velocity increases, dispersion increases through the following relationship relating the average linear velocity (v) to the dispersion coefficient (D) through the dispersivity (α).

$$D = \alpha v + D_{mp} \quad \text{eq. 3}$$

where D_{mp} is the coefficient of molecular diffusion within the porous medium. Values of porous medium molecular diffusion coefficients are lower than free air diffusion coefficients for the same compounds because tortuous pathways through the porous medium increase the path length that a molecule must travel (Millington and Quirk, 1961). Typical values previously estimated for the Bandelier tuff (porosity

40-50%) are on order of $3 \times 10^{-6} \text{ m}^2/\text{s}$. Another approach to calculate porous media diffusion coefficients is to use the Millington-Quirk (1961) formulation where D_{mp} is a function of porosity (ϕ) and air content (θ) as:

$$D_{mp} = \frac{D_{free} \theta_a^{10/3}}{\phi^2} \quad \text{eq. 4}$$

With a free air diffusion coefficient of SF_6 on order of $1 \times 10^{-5} \text{ m}^2/\text{s}$, and assuming air filled porosity in the rubblized basalt to be 35%, this function yields a value of for the molecular diffusion coefficient in the rubblized basalt of $2.5 \times 10^{-6} \text{ m}^2/\text{s}$. From Eq. 3 one can see that the dispersion coefficient can easily increase above pure molecular diffusion as average linear velocity increases.

The average linear velocity of a gas flowing in a porous medium is equal to the volumetric flux (volume per area per time, or volume moving through a window) divided by the porosity (Stauffer, 2006), and represents the average rate at which a molecule moves through the subsurface. Dispersivity in the direction of flow follows a very approximate 1/10 flow length relationship, while dispersivity in the direction perpendicular to flow is often taken to be 1/100 the flow length. This relationship is based on field data showing plumes spread more with longer distance transport (Fetter, 1999).

To calculate possible increased mass transport from dispersion, one needs both an estimate of the velocity of the gas and the dispersivity (Auer et al., 1996). Through simulation, we determined that a longitudinal dispersivity of 1 m led to spreading that could match observations. Also through simulation, using permeability and porosity that fit the pressure response, average linear velocity of the gas near the injection/sampling port can be determined. Figure 6.4-1 shows the dispersion coefficient calculated using simulated volumetric flux and assigned porosity in both the rubblized and massive basalt near the injection port. Although the massive basalt appears to have a very large impact on spreading, the total mass flowing in these layers is limited by the very low assigned porosity of 0.4%. In the rubblized basalt, the much higher porosity (35%) dominates mass transfer. However, even in the high porosity basalt, the dispersion coefficient ranges well above pure diffusive transport ($< 2.5 \times 10^{-6} \text{ m}^2/\text{s}$). Thus, the barometrically pumped gases in the Cerros del Rio basalt are likely seeing 10x to 100x more mixing than standard diffusive theory would predict. With a longitudinal dispersivity of 1 m, Figure 6.4-1 is also the absolute value of the magnitude of the average linear velocity (v). Figure 6.4-2 converts the average linear velocity into more intuitive units of meters per day, showing that gas molecules may be traveling laterally in the rubblized basalt at speeds greater than 10 m/day, with maximum velocities reaching above 20 m/day. Within the massive basalt fractures, estimates of average linear velocity are dramatically higher, with values reaching maximums of nearly 1000 m/day.

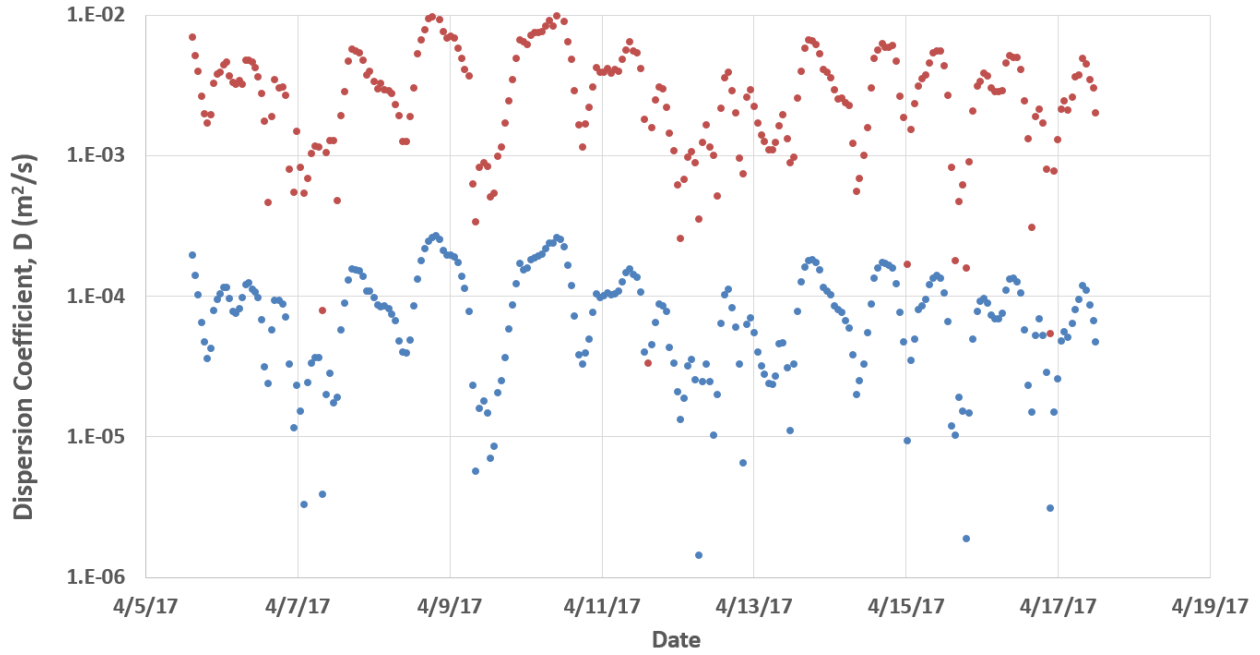


Figure 6.4-1 Dispersion coefficient as a function of time for both the rubblized basalt (blue) and the massive fractured basalt (red).

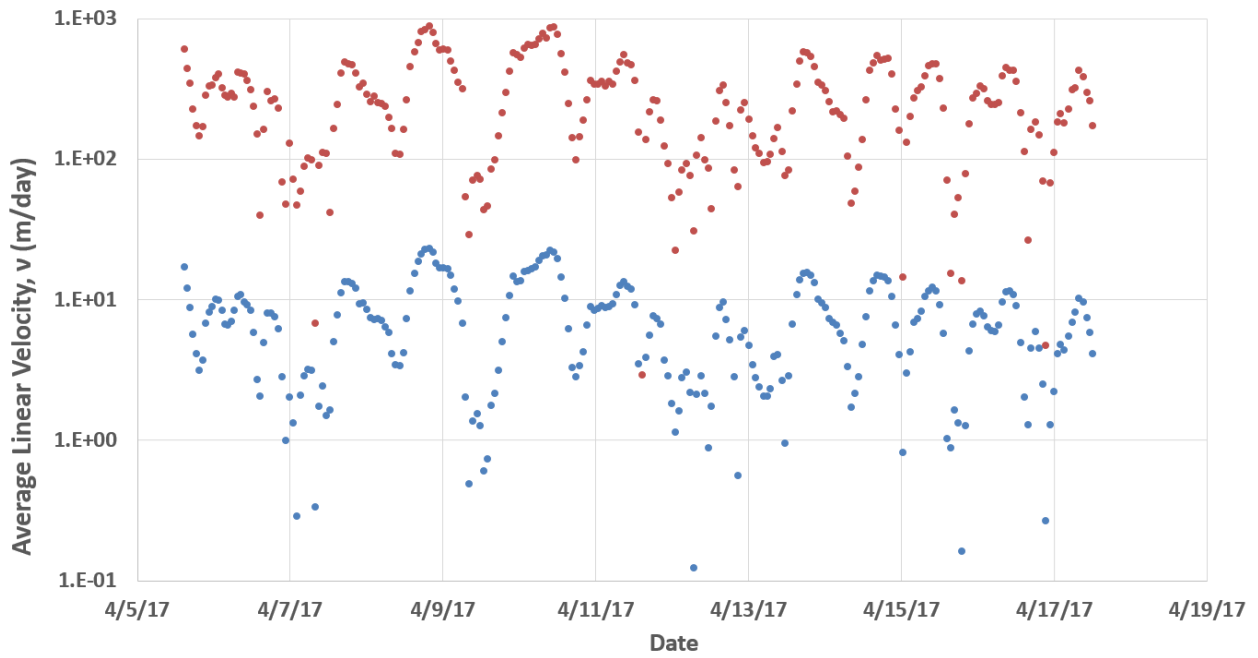


Figure 6.4-2 Average linear velocity as a function of time in the rubblized basalt (blue) and the massive fractured basalt (red).

7 Discussion

7.1 Borehole 54-24399 Data Variability

The recent tracer test, combined with other observations of plume related VOC concentrations in the deep basalt have cause re-examination of our conceptual model for this horizon. Calculations of Tier II screening for the MDA L CME (2011) assumed simple porous medium diffusion using values for the diffusion coefficient unmodified to account for the increased mixing caused by barometric pumping. In the same CME, simulations of transport to the regional aquifer considered accentuated diffusion of up to 10x porous media molecular diffusion (D_{mp}). However, as shown in Figure 4.2-3 through Figure 4.2-5, concentrations 200 ft below the bottom of the Bandelier tuff vary on timescales of hours to days, something that is not predicted in simple diffusion calculations. Further, VOC data collected using SUMMA canisters from the open section of borehole 54-24399 and analyzed using TO-15 laboratory standard methods show similar time varying concentrations (Figure 7.1-1). In Figure 7.1-1 the vertical black line represents the time when the permanent packer was installed in August 2016, and the horizontal orange line shows the Tier I screening level for 1,1,1-TCA. Tier I screening assumes the measured gas phase VOC concentration is in equilibrium with drinking water at the regional aquifer, taking no credit for dilution during transport from the measurement location to the regional aquifer (2011 CME).

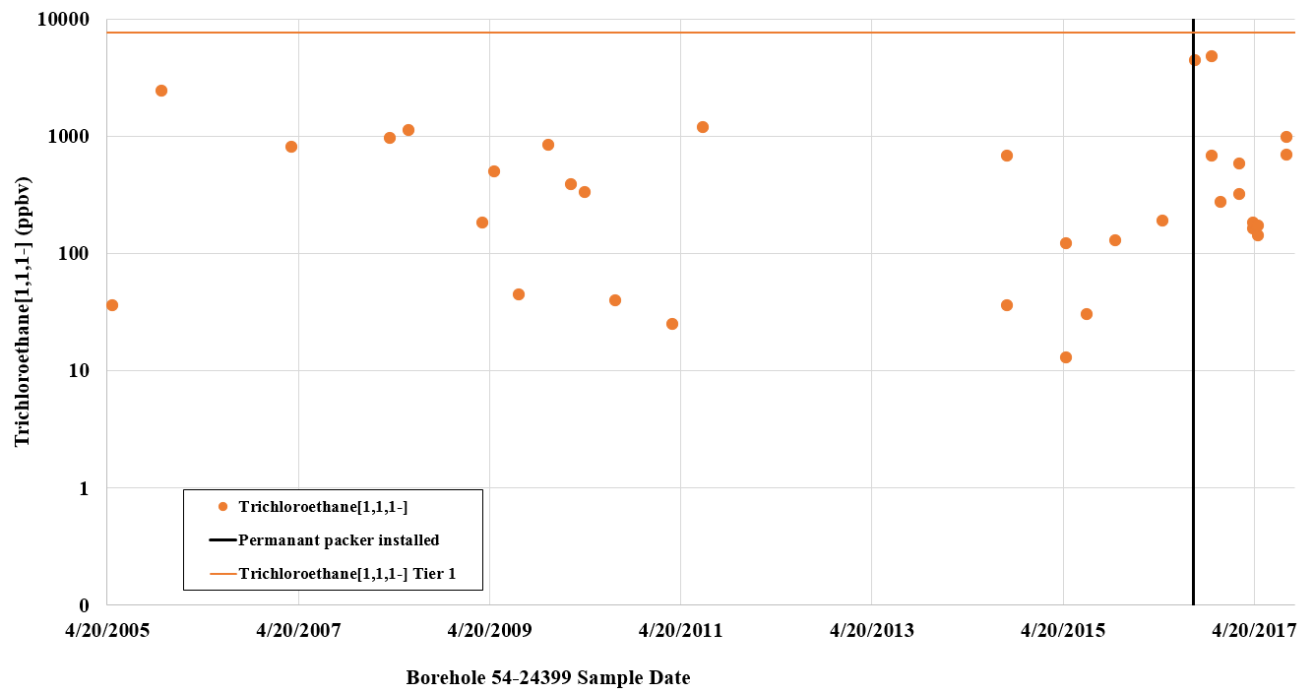


Figure 7.1-1 SUMMA data for 1,1,1-TCA for borehole 54-24399

7.2 Revised Conceptual Model

A revised conceptual model for flow and transport is shown schematically in Figure 7.2-1. In the top figure (A), a barometric low pressure pulls a packet (orange ball outlined in red) of VOC downward from the Bandelier Tuff into the Cerros del Rio basalts.

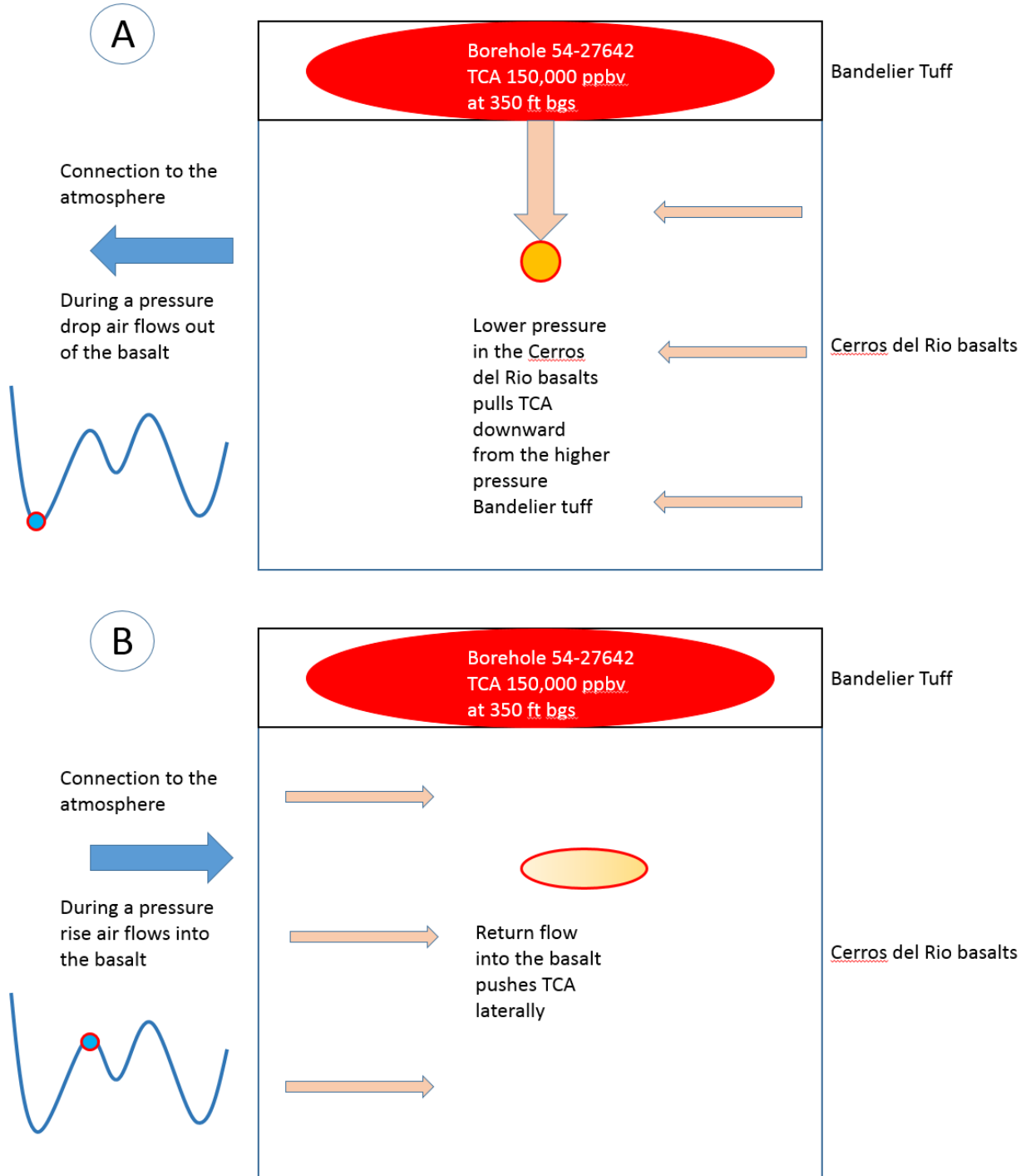


Figure 7.2-1 Conceptual model for transport in the Cerros del Rio Basalt

The downward pressure gradient from the Bandelier Tuff into the basalts develops because the lower permeability in the Bandelier Tuff phase-shifts the pressure low to a later time and a lower amplitude (Figure 1.1-3). As the organic vapor moves vertically downward from the tuff to the basalt, the pressure gradient within the basalt acts to pull the vapors toward the atmospheric connection. Although the figure shows horizontal flow vectors within the basalt, there likely are vertical components to these flow paths caused by the heterogeneity in the layers of rubblized and massive basalt and effects related to the three dimensional atmospheric boundary. As atmospheric pressure rises, flow paths reverse and air flows back into the basalt (B). The packet of higher concentration that was pulled into the basalt during the atmospheric low now is transported laterally, with some possible vertical component. Transport leads to spreading and dispersion of the packet as shown by the stretched and diluted orange oval outlined in red in (B). Longer, deeper lows in barometric pressure should push larger packets of VOC mass into the basalt and, subsequently, be pulled out toward the atmospheric boundary.

This conceptual model allows discrete packets of different concentrations to move through the basalt as suggested by both the INNOVA and SUMMA measurements. The barometric pumping is thus accentuating migration from the Bandelier Tuff into the Cerros del Rio basalts. However, the impact of the barometric pumping on the rate of transport of VOCs to the regional aquifer through the basalts is less definitive. In the end member situation where barometric flow is purely horizontal, the high average linear velocities shown in Figure 6.4-2 would tend to smear the plume laterally, with the possibility that a sizable fraction of any individual VOC packet being exhausted to the atmosphere in a relatively short period of time.

8 References

The following list includes all documents cited in this report. Parenthetical information following each reference provides the author(s), publication date, and ER ID or ESH ID. This information is also included in text citations. ER IDs were assigned by the Environmental Programs Directorate's Records Processing Facility (IDs through 599999), and ESH IDs are assigned by the Environment, Safety, and Health (ESH) Directorate (IDs 600000 and above). IDs are used to locate documents in the Laboratory's Electronic Document Management System and, where applicable, in the master reference set.

Copies of the master reference set are maintained at the NMED Hazardous Waste Bureau and the ESH Directorate. The set was developed to ensure that the administrative authority has all material needed to review this document, and it is updated with every document submitted to the administrative authority. Documents previously submitted to the administrative authority are not included.

- Auer, L.H., N.D. Rosenberg, K.H. Birdsell, and E.M. Whitney, November 1996. "The Effects of Barometric Pumping on Contaminant Transport," *Journal of Contaminant Hydrology*, Vol. 24, No. 2, pp. 145–166. (Auer et al. 1996, 069793)
- Jordon, A.J., P.H. Stauffer, E. E. Knight, E. Rougier¹, and D.N. Anderson, Radionuclide Gas Transport through Nuclear Explosion-Generated Fracture Networks, (2015). *Scientific Reports*, 5:18383 | DOI: 10.1038/srep18383.
- Jordon, A.J., J.K. MacCarthy, P.H. Stauffer, G.A. Zvoloski, M.A. Person, D.N. Anderson, (2104). Uncertainty in Prediction of Radionuclide Gas Migration from Underground Nuclear Explosions, *Vadose Zone J.*, Vol 13 (10). October 2014. doi:10.2136/vzj2014.06.0070.
- Kestin, J., et al., *J. Phys. Chem. Ref. Data*, 13, 229, 1984.
- LANL (Los Alamos National Laboratory), September 2011. "Corrective Measures Evaluation Report for Material Disposal Area L, Solid Waste Management Unit 54-006, at Technical Area 54, Revision 2," Los Alamos National Laboratory document LA-UR-11-4798, Los Alamos, New Mexico. (LANL 2011, 205756)
- LANL (Los Alamos National Laboratory), September 2014. "Interim Measures Work Plan for Soil-Vapor Extraction of Volatile Organic Compounds from Material Disposal Area L, Technical Area 54, Revision 1," Los Alamos National Laboratory document LA-UR-14-26472, Los Alamos, New Mexico. (LANL 2014, 261843)
- LANL (Los Alamos National Laboratory) 2016. Work Plan for a Tracer Test at Material Disposal Area L, Technical Area 54, Los Alamos National Laboratory Document LA-UR 16-24628.
- Marrero, T. R., and Mason, E. A., *J. Phys. Chem. Ref. Data*, 1, 1, 1972.
- Millington, R.J., and J.P. Quirk. 1961. Permeability of porous solids. *Trans. Faraday Soc.* 57:1200–1207. doi:10.1039/tf9615701200
- Neeper, DA; and Stauffer, P. (2012A). Transport by Oscillatory flow in Soils with Rate-limited Mass Transfer I. Theory, *Vadose Zone J*, doi:10.2136/vzj2011.0093.
- Neeper, DA; and Stauffer, P. (2012B). Transport by Oscillatory flow in Soils with Rate-limited Mass Transfer II. Field Experiment, *Vadose Zone J*, doi:10.2136/vzj2011.0094.

- Neeper, D.A., 2002. "Investigation of the Vadose Zone Using Barometric Pressure Cycles," *Journal of Contaminant Hydrology*, Vol. 54, pp. 59-80. (Neeper 2002, 098639)
- Neeper, D.A., 2003. "Harmonic Analysis of Flow in Open Boreholes Due to Barometric Pressure Cycles," *Journal of Contaminant Hydrology*, Vol. 60, pp. 135-162. (Neeper 2003, 098640)
- Stauffer, P.H. K.H. Birdsell, and W.J. Rice (2011). 3-D Model Validation in Support of Site Closure, Material Disposal Area L, Los Alamos, NM, Waste Management 2011, Phoenix Arizona, March 7-11.
- Stauffer, P.H., J.K. Hopkins, T. Anderson, and J. Vrugt, July 11, 2007. "Soil Vapor Extraction Pilot Test at Technical Area 54, Material Disposal Area L: Numerical Modeling in Support of Decision Analysis," Los Alamos National Laboratory document LA-UR-07-4890, Los Alamos, New Mexico. (Stauffer et al. 2007, 097871)
- Stauffer, P.H. (2006). Flux Flummoxed: A Proposal for Consistent Usage, *Ground Water*, V. 44(2): 125-128.
- Stauffer, P.H., K.H. Birdsell, M.S. Witkowski, and J. K. Hopkins (2005), Vadose Zone Transport of 1,1,1-Trichloroethane: Conceptual Model Validation through Numerical Simulation, *Vadose Zone Journal* 2005 4: 760-773.
- Storn, R. & Price, K. *Journal of Global Optimization* (1997) 11: 341.
<https://doi.org/10.1023/A:1008202821328>

9 Appendix A: FEHM Input Files

This section presents selected FEHM input files for the best fit simulation of pressure propagation and tracer transport. The best fit tracer simulation is located in:

```
/scratch/er/stauffer/L/2014_SVE_runs/Basalt_tracer/2017_April_Simulated/April5-17_tracer_tet_20m_tB2-0.1C-well
```

The rest of the files to run these simulations can be found in:

```
/scratch/er/stauffer/L/2014_SVE_runs/Basalt_tracer and subdirectories therein.
```

9.1 FEHM Input Deck

title: Area L Pressure fixed at 2100m inj at 1100m

text

Basalt Tracer Test

airwater

3

20 0.08

#----- ZONE FOR Borehole and BOUN

massive basalt is everything else

21 top rubble zone 6 m 1 meter!!

22 bot rubble zone 0-1 m 1.5 meters!!

55 is borehole - REMOVED IN THIS VERSION

66 is upper port

67 is lower port

99 is radial boundary

zone

file

```
../Grid_2.5km_box/rubble_inj_prod_2101m_ATM-B.zone
```

#-----

rlp

-1 0.0 1.0 1.e-5 0.001

1 0 0 1

Well is 208279 to 208319 40 nodes (8 x 5)

Narrower total well, 0.25 m radius (half of a 1m3 block)

well

wellmodel

1 1

1 4 9 0

1 10. 1100. 8. 0.07 0. 0. 0.25

-9 10. 1100. 0. 0.07 0. 0. 0.25

wellend

#-----

top of the well above shallow sample port is blocked off.

rock

1 0 0 1800. 1200. 0.004

-21 0 0 1800. 1200. 0.35

```

-22 00 1800. 1200. 0.35
-66 00 1800. 1200. 0.35
-67 00 1800. 1200. 0.35
10343 10343 1 1800. 1200. 0.35
-99 00 1800. 1200. 0.35
208279 208284 5 1800. 1200. 0.00001
208289 208319 5 1800. 1200. 0.9999

```

dual material Rubble + Massive Basalt 4mm crack in massive perm

```

1 00 5.333e-9 5.333e-9 5.333e-9
-21 00 0.77e-8 0.77e-8 0.77e-8
-22 00 0.77e-8 0.77e-8 0.77e-8
-66 00 0.77e-8 0.77e-8 0.77e-8
-67 00 0.77e-8 0.77e-8 0.77e-8
10343 10343 1 0.77e-8 0.77e-8 0.77e-8
-99 00 0.77e-8 0.77e-8 0.77e-8
208279 208284 5 1.e-29 1.e-29 1.e-29
208289 208319 5 1.e-4 1.e-4 1.e-4

```

#-----

pres

```
1 0 0 0.080461 0.01 2
```

3.33e-5 kg/s = 2 L/min +outflow -inflow

boun

model 1

ti

5

```
0.0 31.01132 31.0243 31.02429 50.00
```

sa

```
0.0 -3.33e-5 0.0 3.33e-5 3.33e-5
```

model 2

ti

5

```
0.0 31.0104 31.0243 31.0396 50.00
```

sa

```
0.0 3.33e-6 -3.33e-5 3.33e-6 3.33e-6
```

```
208289 208289 1 1
```

```
208319 208319 1 2
```

#----- TIME

time

```
1.e-2 42.8958 10000 10 2016 2
```

#-----

ctrl

```
-3 1.e-07 40 100 gmres
```

```
1 00 2
```

```
0 0 0 0
```

```
1.0 0 1.0
```

```
16 1.4 1.e-9 0.0052
```

```

0 +1
iter
1.e-5 1.e-5 1.e-5 -1.e-5 1.2
0 0 0 19400.
sol
+1 -1
node
10
208289 114484 149195 208284 208294 208299 208304 208309 208314 208319
#-----
hist
press
vectors
concentration
end
#----- CONT
cont
avsx 1000000 5.
press
conc
veloc
material
geo
sat
vapor
liquid
endavs
#----- BOUN
boun
file
../Grid_4km_box/2017_March5_April-17_press.boun
#----- Tracer
# ZONE 66 = TOP 567.
# ZONE 67 = BOTTOM 588.
trac
0 1 1.e-7 1.0
31.0104 42.8958 1.e8 1.e8
20 1.4 1.e-5 0.01 10
1
ldsp
-1
0 0 0 1 3.e-6 1. 0.1
0 0 0 1 3.e-15 1. 0.1

1 0 0 1
208279 208284 5 2

1 0 0 1.e-19
208289 208319 5 0.03605

-99 0 0 -1.e-19 0. 30000.
stop

```

9.2 Zone file for the location of the atmospheric boundary and basalt regions

zone

21

```
0.0 20.0 20.0 0.0 0.0 20.0 20.0 0.0
0.0 0.0 4000.0 4000.0 0.0 0.0 4000.0 4000.0
5.5 5.5 5.5 5.5 6.0 6.0 6.0 6.0
```

22

```
0.0 20.0 20.0 0.0 0.0 20.0 20.0 0.0
0.0 0.0 4000.0 4000.0 0.0 0.0 4000.0 4000.0
0.0 0.0 0.0 0.0 1.5 1.5 1.5 1.5
```

66

```
9.99 10.1 10.1 9.99 9.99 10.1 10.1 9.99
1099.9 1099.9 1100.1 1100.1 1099.9 1099.9 1100.1 1100.1
5.5 5.5 5.5 5.5 6.0 6.0 6.0 6.0
```

67

```
9.99 10.1 10.1 9.99 9.99 10.1 10.1 9.99
1099.9 1099.9 1100.1 1100.1 1099.9 1099.9 1100.1 1100.1
0.0 0.0 0.0 0.0 0.5 0.5 0.5 0.5
```

99

```
0.0 20.0 20.0 0.0 0.0 20.0 20.0 0.0
2101.0 2101.0 2102.0 2102.0 2101.0 2101.0 2102.0 2102.0
8.0 8.0 8.0 8.0 0.0 0.0 0.0 0.0
```

Stop

9.3 FEHMN.FILES

root: run

input: run.dat

output: run.out

grida: ../../Grid_2.5km_box/tet.fehmn

stor: ../../Grid_2.5km_box/tet.stor

error: run.err

check: run.chk

nopf: ../../Grid_2.5km_box/nop-well.temp

rsti: ../March5_April5__20m_press_only_o2B-well/run_April_5.ini

rsto: run.fin

all

0

10 Appendix B: Tracer Test Implementation Details

Details for a Tracer Test at Material Disposal Area L, Technical Area 54

This section presents the physical components, connections, and operation steps needed to implement a SF₆ tracer test in deep borehole 54-24399 at Material Disposal Area (MDA) L. The detailed descriptions presented herein supplement the 'Work Plan for Tracer Test at MDA L (EP2016-0098). Sampling boreholes 54-01015 and 54-01016 is covered in the SOP for subsurface vapor sampling (ER-SOP-20294, R0).

1) Equipment List

- Weather-proof box to hold the sampling equipment
- INNOVA Photoacoustic Gas Monitor with SF₆ monitoring capability
- Nitrogen tank used to inflate the installed borehole packer
- Pressure transducer used to measure surface atmospheric pressure
- Data logger to record pressure from both the surface and subsurface pressure transducers.
- Desiccant (e.g. Drierite, anhydrous calcium sulfate, CaSO₄)
- A diaphragm pump capable of pulling 1 L/min from the deep sampling port
- 10 L Carboy
- Power cord (heavy duty)
- Power strip (6 outlets GFCI)
- Inverter to convert 120V to 12V to provide power to the pump

- Tedlar® bags for collecting samples for high precision laboratory analysis
- A tracer injection/sample collection port
- Tubing to and connectors to connect the gas sampling port on the wellhead to the desiccant, then to the pump, then to the 10 L carboy
- Tubing to connect the carboy to the tracer injection/sample collection port
- Tubing to connect the tracer injection/sample collection port to the injection port on the wellhead
- Tubing to pull samples from the primary injection/sampling loop (l,m,n) into the INNOVA sampling bypass and connect to the INNOVA inlet port
- Tubing to connect the INNOVA exhaust back into the main injection/sample collection loop

2) Equipment Connections (Figure 1)

- Swagelok® fitting on tubing connecting the sampling port on the wellhead to the pump
- Open tubing connecting to the inlet side of the pump
- Open tubing connecting to the outlet side of the pump
- A three way Swagelok® fitting allowing the INNOVA sampling bypass to pull gas from the primary injection/sampling loop.
- An open tubing connector to connect to the inlet of the INNOVA
- An open tubing connector to connect to the exhaust of the INNOVA
- A three way Swagelok® fitting allowing the INNOVA sampling bypass to reintroduce INNOVA exhaust gas into the primary injection/sampling loop.
- Swagelok® fittings on both ends of the tubing connecting (g) to (i)
- A three way Swagelok® fitting allowing tracer to be injected into the line or analytical Tedlar® bag samples to be pulled
- Swagelok® fittings on both ends of the tubing connecting (i) to the injection port on the wellhead

3) Order of Operations

- a. Connect tubing between the wellhead sampling port and the desiccant, pump, and carboy
- b. Connect tubing from carboy to Swagelok® fitting 2-d
- c. Connect tubing from fitting 2-d to fitting 2-g
- d. Connect tubing from fitting 2-g to fitting 2-i
- e. Connect tubing between the wellhead injection port and fitting 2-i
- f. Connect INNOVA to fitting 2-d
- g. Connect the exhaust port of the INNOVA to fitting 2-g
- h. Connect a nitrogen bottle to the nitrogen port on the wellhead
- i. Connect the cable from the subsurface pressure transducer at the wellhead to the data logger
- j. Connect the surface pressure transducer cable to the data logger
- k. Connect the power cord to power
- l. Connect the power strip to the power cord
- m. Connect the inverter to the power strip
- n. Connect the data logger to the power strip
- o. Turn on the data logger
- p. Inflate the packer (record pressure on Attachment 1)
- q. Connect power cord from pump to inverter and turn on pump
- r. Turn on the INNOVA (record initial measurements on Attachment 2)
- s. Record INNOVA measurements until CO₂ stabilizes
- t. Attach tracer injection bag to fitting 2-i
- u. Inject tracer into the continuous loop by squeezing bag
- v. Collect samples from fitting 2-l (see Table 1)